

This is an Open Access document downloaded from ORCA, Cardiff University's institutional repository:<https://orca.cardiff.ac.uk/id/eprint/95292/>

This is the author's version of a work that was submitted to / accepted for publication.

Citation for final published version:

Qin, Yongpeng, Alves, Tiago Marcos , Constantine, Jose Antonio and Gamboa, Davide 2016. Quantitative seismic geomorphology of a submarine channel system in SE Brazil (Espírito Santo Basin): Scale comparison with other submarine channel systems. *Marine and Petroleum Geology* 78 , pp. 455-473.
10.1016/j.marpetgeo.2016.09.024

Publishers page: <http://dx.doi.org/10.1016/j.marpetgeo.2016.09.024>

Please note:

Changes made as a result of publishing processes such as copy-editing, formatting and page numbers may not be reflected in this version. For the definitive version of this publication, please refer to the published source. You are advised to consult the publisher's version if you wish to cite this paper.

This version is being made available in accordance with publisher policies. See <http://orca.cf.ac.uk/policies.html> for usage policies. Copyright and moral rights for publications made available in ORCA are retained by the copyright holders.



Quantitative seismic geomorphology of a submarine channel system in SE Brazil (Espírito Santo Basin): Scale comparison with other submarine channel systems

Yongpeng Qin ^a, Tiago M. Alves ^a, Jose Constantine ^b, Davide Gamboa ^c

^a 3D Seismic Lab, School of Earth and Ocean Sciences, Cardiff University, Main Building, Park Place, Cardiff, CF10 3AT, United Kingdom

^b Geosciences Department, Williams College, Clark Hall, 947 Main Street, Williamstown, MA, 01267, United States

^c British Geological Survey e Cardiff Office, Columbus House, Village Way, Greenmeadow Springs, Tongwynlais, Cardiff, CF15 7NE, United Kingdom

Abstract

Detailed morphological analyses of a Pleistocene-Holocene submarine channel system in terms of its hierarchical framework, were carried out using a 3D seismic volume from offshore Espírito Santo, SE Brazil. The channel morphology shows marked variations, with five segments (Segments a to e) being identified along its full length. For example, the cross-sectional area of the channel decreases by a factor of 70 from Segment a to Segment c, and is then followed by a nearly four-fold increase from Segment c to Segment d. The significant changes in channel morphology relate to temporal and spatial variations in flow volume within the channel. In the same channel system, the valley reveals three distinct segments (Segments A to C), with similar aspect ratios but marked variations in morphology along the valley distance. Valley morphological changes are chiefly affected by erosional processes. Segment B is characterised by the largest valley-base width, valley width, and cross-sectional area compared to the other two segments. Valley enlargement in Segment B results from relatively high degrees of lateral channel migration and associated cut bank erosion, leading to the widening of the valley, especially the valley base. In Segment C, the valley is characterised by inner bank erosion in the form of shallow-seated mass failures, which only enlarged the upper part of the valley wall. The spatial variations in both channel and valley morphology documented here suggest an important role of local factors (e.g. salt diapirs, tributaries, overbank collapse) in the development of channel systems. Hence, the morphological analyses developed in this work provide an effective tool for studying channels and valleys on continental slopes around the world.

1. Introduction

Submarine channels are major conduits for sediment transported from continental shelves to abyssal plains, and their deposits comprise important reservoirs in deep-water basins when filled with sand- or silt-prone sequences (Mayall and Stewart, 2000; Mayall et al., 2006; Wynn et al., 2007). To better organize and compare architectural elements associated with submarine channels, several hierarchical frameworks have been proposed in the literature (Gardner and Borer, 2000; Champion et al., 2000; Sprague et al., 2002, 2005). Stratigraphic elements of multiple scales such as channels, channel complexes and channel complex sets have been comprehensively documented in previous studies (e.g. Gardner and Borer, 2000; Gardner et al., 2003; Abreu et al., 2003; Deptuck et al., 2003; McHargue et al., 2011; Di Celma et al., 2011; Thomas and Bodin, 2013; Bain and Hubbard,

2016).

In recent years, high-resolution seismic and bathymetric data have been used in morphological studies of submarine channel systems in regions such as the Amazon fan (Flood and Damuth, 1987; Pirmez and Flood, 1995), offshore Gabon (Wonham et al., 2000), Zaire fan (Babonneau et al., 2002), Niger delta (Deptuck et al., 2007; Jobe et al., 2015) and Caribbean Sea (Wood and Mize-spansky, 2009). However, the majority of previous studies have been focused on either the channel scale (e.g. Flood and Damuth, 1987; Clark et al., 1992; Pirmez and Flood, 1995; Babonneau et al., 2002; Antobreh and Krastel, 2006; Gee et al., 2007; Estrada et al., 2005; Clark and Cartwright, 2009; Peakallet al., 2012; Kolla et al., 2012; Georgiopoulou and Cartwright, 2013; Jobe et al., 2015) or the channel-complex scale (e.g. Catterall et al., 2010; Wood and Mize-spansky, 2009), with few published papers addressing the morphological characteristics of both scales in the same channel system (Wonham et al., 2000; Deptuck et al., 2007).

Outcrops of submarine channel systems have shown stratigraphic elements of distinct sizes, from small-scaled channel elements to large-scaled channel complexes and channel complex sets (e.g. Grecula et al., 2003; Lien et al., 2003; Vigorito et al., 2006; Hubbard et al., 2008, 2009, 2014; Thomas and Bodin, 2013; Gamberi et al., 2013; Macauley and Hubbard, 2013; Bain and Hubbard, 2016). They have revealed the size of channel complexes and channel complex sets to be similar to the seismic scale, allowing for comparisons between seismic and outcrop data (e.g. Lien et al., 2003; Vigorito et al., 2006; Thomas and Bodin, 2013; Bain and Hubbard, 2016). However, to further bridge the gap between seismic and outcrop studies, new morphological data are increasingly needed from high-quality seismic volumes, especially when addressing spatial changes in channel-associated stratigraphic elements.

This work focuses on a submarine channel system, named Rio Doce channel system, developed on the continental slope of SE Brazil (Fig. 1). It documents the morphological characteristics of the channel system at both channel and valley (i.e. channel complex) scales, and is followed by a scale comparison with other channel systems in terms of their hierarchical framework.

2. Terminology

Three main types of morphological features (i.e. channel, channel belt and valley) and their deposits are defined in the following section (Fig. 2).

The term submarine channel, or channel as used herein, defines V- or U-shaped negative features on the seafloor (Fig. 2c). Buried channels refer to sub-surface channels filled by sediments, a character distinguishing them from channels on the seafloor. Depositional units in buried channels comprise the channel fill. The lowest point in a channel is defined as the channel thalweg. Submarine channels correspond to channel elements in the established stratigraphic hierarchical frameworks (Sprague et al., 2002; Abreu et al., 2003; McHargue et al., 2011; Thomas and Bodin, 2013).

Channel belt is defined as a morphological feature on the seafloor. It is composed of channel and terraces (Fig. 2d). A terrace is defined as a topographic flat bordering a channel within the channel belt (Babonneau et al., 2004). Terraces are generated by multiple mechanisms such as entrenchment, bank failure, deposition of inner/internal levees, lateral channel migration, and meander cut-offs (Babonneau et al., 2004; Deptuck et al., 2003; Hansen et al., 2015). The term channel belt is used in multiple studies (Deptuck et al., 2003; Posamentier, 2003; Catterall et al., 2010; Kane and Hodgson, 2011; Gamberi et al., 2013; Hansen et al., 2015). The architectural

features in these studies correspond to what this paper defines as the valley.

Valley is an architectural element of higher order than the channel (Samuel et al., 2003; Kolla, 2007; Janocko et al., 2013). It comprises the sub-surface valley fill and the channel belt (Fig. 2e). The valley corresponds to a channel complex when considering a stratigraphic hierarchical framework, as both are composed of two or more genetically related channel-fill episodes (Sprague et al., 2002; Abreu et al., 2003; McHargue et al., 2011; Thomas and Bodin, 2013). The valley is formed by lateral migration and vertical stacking of a single channel element (e.g. Samuel et al., 2003; Deptuck et al., 2003; Babonneau et al., 2004; Kolla, 2007; Janocko et al., 2013), and has a composite erosional surface consisting of a valley base and adjacent valley walls (erosional fairway *sensu* Deptuck et al., 2003; Catterall et al., 2010; master erosion/incision surface *sensu* Gee et al., 2007; channel-belt erosion surface *sensu* Kane and Hodgson, 2011; bounding erosion surface *sensu* Hansen et al., 2015) (Fig. 2e). The lowest point of the valley's erosional surface is the valley thalweg.

Levees are overbank deposits with gull-wing geometries that converge away from the channel thalweg. External levees (outer levees *sensu* Deptuck et al., 2003, 2007; master-bounding levees *sensu* Posamentier, 2003) and internal levees (inner levee *sensu* Deptuck et al., 2003, 2007) are used to differentiate levees deposited outside and inside the valley (Kane and Hodgson, 2011).

The term channel system is used here to refer to all genetically related morphological and depositional components. It is defined by the valley (or channel complex) plus the external levees confining the valley (Fig. 2b). Two or more genetically related channel systems comprise a channel complex set.

3. Geological setting

3.1 Tectono-sedimentary evolution of the Espírito Santo Basin

The Espírito Santo Basin (ESB) is located on the SE Brazil continental margin between the Abrolhos Bank and the Campos Basin (Fig. 1a). The width of the ESB's continental shelf increases from 50-60 km in the south to 240 km on the Abrolhos Bank in the north (Bastos et al., 2015). The modern shelf break varies in depth from 40 to 80 m (Knoppers et al., 1999; Bastos et al., 2015).

Four tectono-sedimentary stages have been interpreted in the ESB; pre-rift, syn-rift, transition and drift stages (Fig. 3) (Ojeda, 1982). The pre-rift stage spans the Late Jurassic to Early Cretaceous and records the deposition of fluvial-lacustrine sediments in basins dominated by moderate fault-related subsidence (Ojeda, 1982; Chang et al., 1992). The syn-rift stage developed from the Late Berriasian to Early Aptian and was dominated by intense tectonic subsidence. This stage records the widespread formation of rift basins in the ESB, in which deposition of fluvial and lacustrine sediments took place (Fig. 3). Magmatic activity also occurred at this stage (Fig. 3), resulting in basaltic and andesitic volcanism (Ojeda, 1982). An angular unconformity marks the boundary between the syn-rift and post-rift stages (Chang et al., 1992).

Following syn-rift tectonics, the transitional stage spanned the Middle Aptian to Late Aptian/Early Albian, in which the deposition of thick evaporite sequences and marine carbonates predominated (Ojeda, 1982).

The drift phase ranges in time from Late Aptian/Early Albian to the present-day, and is characterised by the deposition of open-marine strata (Ojeda, 1982; Chang et al., 1992) (Fig. 3).

Strata deposited in this phase are divided into two megasequences: earlydrift transgressive and late-drift regressive megasequences (Mohriak, 2003; Fiduk et al., 2004) (Fig. 3). The transgressive megasequence consists of Albian carbonate platforms accumulated below muddy and sandy turbidites, and marks a general deepening-upwards trend towards the end of the Cretaceous (Davison, 1999; Fiduk et al., 2004; Alves et al., 2009). The regressive megasequence marks the reactivation of rift structures and episodic magmatic activity (Demercian et al., 1993; Cobbold et al., 2001; Mohriak et al., 2008), and is associated with the emplacement of the Abrolhos Bank to the north of the study area (Cordani, 1970). A large amount of sediments sourced from the Abrolhos Bank and onshore rivers were transported downslope by submarine canyons and channels during the regressive megasequence (Bruhn and Walker, 1997; Davison, 1999).

3.2 Salt tectonics in the Espírito Santo Basin

Salt tectonics has been active in the ESB since the Albian (Fiduk et al., 2004). The main triggers for salt tectonics in the region are gravitational gliding and differential loading by overburden rocks of variable thickness (Demercian et al., 1993; Fiduk et al., 2004). As a result, three tectonic domains are interpreted in the ESB, each showing different salt structural styles (Fiduk et al., 2004) (Fig. 4). The proximal domain is characterised by salt rollers and rafts. Salt deformation in this domain is dominated by extensional processes (Demercian et al., 1993; Fiduk et al., 2004; Alves, 2012). In the transitional mid-slope domain, where the study area is located, salt diapirs predominate (Fiduk et al., 2004). Basinwards, the compressional domain is dominated by allochthonous salt canopies, tongues and overhangs (Fiduk et al., 2004; Mohriak et al., 2008).

In the study area, several salt diapirs are rooted in two NW-SE trending salt ridges (Gamboa and Alves, 2015). With the exception of D2, all salt diapirs have a seafloor expression at present (Fig. 1b). Various architectural elements, such as mass-transport deposits (MTDs), turbidite lobes, submarine canyons and channels are observed within a salt-withdrawal basin delimited by salt diapirs D1 to D6 (Gamboa and Alves, 2015). These elements are strongly influenced by the relative location and movement of the salt diapirs (Baudon and Cartwright, 2008; Alves et al., 2009; Gamboa et al., 2012; Gamboa and Alves, 2015). Topographic confinement created by salt diapirs is reflected by changes in channel density, geometry and sinuosity (Alves et al., 2009; Gamboa et al., 2012). As an example, channel density decreases from the unconfined region to the topographically confined region (Gamboa et al., 2012).

3.3. Rio Doce Canyon system in the Espírito Santo Basin

The Rio Doce Canyon system, defined as a set of stacked Eocene to recent submarine channels developed in the northern part of the ESB, is one of the most important depositional features offshore SE Brazil (Fiduk et al., 2004). The sediment source of this canyon system is affected by longshore drifts, which play an important role in distributing sediment on the continental shelf and slope of SE Brazil (Dominguez et al., 1992; Martin and Suguio, 1992). At least three major channel events have been identified within the Rio Doce Canyon system (Fig. 5): (1) an Eocene channel system controlled by adjacent faults generated on the flanks of growing diapirs (Alves et al., 2009), (2) a Miocene channel system with multiple laterally shifting channels, and (3) a Pliocene-Quaternary channel complex set confined by salt diapirs (Gamboa et al., 2012) (Fig. 5). The studied

late Pleistocene-Holocene channel system belongs to the Pliocene-Quaternary channel complex set bounded at its base by an intra-Pliocene unconformity of regional expression (França et al., 2007) (Fig. 5).

4. Data and methodology

4.1. Seismic dataset

The interpreted 3D seismic volume is located in the northern part of the ESB (Fig. 1a). The seismic data were acquired by a dual airgun array and a 6 x 5700 m array of streamers. The survey has a bin spacing of 12.5 by 12.5 m and a 2 ms vertical sampling interval. Data processing included resampling, spherical divergence corrections, and zero-phase conversions undertaken prior to stacking, 3D prestack time migration using the Stolt algorithm, and one-pass 3D migration. The vertical resolution of the data is ~10 m at the depth of analysis in this study, based on a dominant frequency of 40 Hz and a P-wave velocity of 1600 m/s for near-seafloor strata. A water-column velocity of 1480 m/s was used for time-depth conversions of the seafloor. The polarity of data is SEG normal i.e., positive amplitude reflections (red) on the seismic profiles represent an increase in acoustic impedance (Fig. 2a).

4.2. Morphological analyses of the channel system

The mapping of the seafloor and channels followed a line-by-line interpretation combined with 3D auto-tracking. The quantitative analyses of the channel system followed the methods of Deptuck et al. (2007) and included channel and valley measurements (Fig. 6).

Channel measurements included the depth of channel thalweg and channel bank below sea level, channel height, width of channel floor and channel, aspect ratio (width/height) and cross-sectional area (CSA) (Fig. 6c). These parameters were measured in equally spaced cross-sections oriented perpendicularly to the channel axis line. The channel CSA was measured at 1-km intervals and other parameters were measured at 125-m intervals. Channel gradient was calculated based on thalweg depth changes along the channel distance.

Valley measurements were conducted at cross-sections perpendicular to the valley axis. The parameters measured include the depth of valley thalweg and valley wall below sea level, valley height, width of valley base and valley, the aspect ratio (width/height) and CSA of the valley (Fig. 6d). The valley CSA was measured at 1-km intervals and other parameters were measured at 65-m intervals. The gradients of the valley thalweg (valley gradient) and the valley walls were calculated based on measurements of depth along the valley.

5. Seafloor morphology

The study area is located on the southern flank of the Abrolhos Bank, a bathymetric feature that is associated with a unique slope configuration in the ESB (Fig. 1a). The presence of the Abrolhos Bank forces a shift in the orientation of the continental shelf, which changes from NE striking to the southwest to ENE striking in the northeastern part of the ESB. This change results in two different slope trends in the study area (Fig. 1b). The western half of study area displays a

decreasing slope from 8° in the northwest to 1° in the southeast, whereas the eastern part shows a gentler slope ranging from 1° to 2° (Figs. 1b and 7). The seafloor is also affected by growing salt diapirs, and in some areas, the slope angle decreases to nearly 0° (Fig. 7).

Three slope regions have been defined based on the degree of confinement imposed by salt diapirs deforming the seafloor (Gamboa et al., 2012) (Fig. 8). The pre-confluence slope (Zone 1) is relatively unconfined and shows a variety of erosional features such as gullies, channels, irregular depressions and headwalls of mass-wasting events (Fig. 8). The confluence region (Zone 2) presents a relatively higher topographic confinement when compared to Zone 1 due to the presence of salt diapirs D2, D3, D5 and D6. As a result, turbidity flows sourced from upslope are diverted by these salt diapirs, as shown by the shift in orientation of the two tributaries in the seafloor channel (Figs. 8 and 9). For example, the pathway of the east tributary changes from NNE-SSW in Zone 1 to NE-SW in Zone 2 due to the presence of salt diapir D5 (Fig. 9). A distinct confluence point for two Miocene tributaries has been observed in the same region (Gamboa et al., 2012), suggesting that the present-day slope configuration was established in the Miocene. Downslope from the post-confluence region (Zone 3), the seafloor becomes less confined after diapirs D2 and D5, and it is relatively smooth with fewer erosional features (Fig. 8).

6. Morphological analyses of the late Pleistocene-Holocene channel system

The late Pleistocene-Holocene channel system is only partially filled, and includes a sinuous channel on the modern seafloor (Figs. 8 and 9). The seafloor channel comprises two upslope tributaries in Zone 1 and a post-confluence channel downslope in Zones 2 and 3 (Fig. 9). The continuity of sedimentary fill patterns between the east tributary and the post-confluence channel, as well as the continuity of the channel thalweg, indicate that these two channel segments constitute the main flow pathway at present (Gamboa et al., 2012). Other small tributaries connected to the east tributary are also observed on the seafloor (Fig. 9). Both west and east tributaries change their orientation in the pre-confluence region, and are diverted into the confluence region due to salt diapirs (Fig. 9). The general orientation of the channel changes to nearly NS until the southern boundary of the seismic volume is reached (Fig. 9).

The dominant flow pathway (east tributary and post-confluence channel) is the focus of the following sections (Fig. 9). Along that pathway, the channel system is divided into different segments (Fig. 10) based on the morphological analyses conducted at channel (Fig. 11 and Table 1) and valley scales (Fig. 12 and Table 2).

6.1. Quantitative channel analyses

The dominant pathway of the seafloor channel is 42 km-long within the seismic dataset. It starts from a water depth of ~1000 m, down to ~1700 m at the southern edge of the seismic volume. The channel shows marked variations in its morphology (Fig. 11 and Table 1). Five distinct segments (Segments a to e) are recognized based on their morphological changes (Figs. 10 and 11, Table 1).

6.1.1. Depth profiles of channel thalweg and channel bank, and channel height profile

The depth profile of the channel thalweg shows an exponential trend and is divided into three

intervals based on the observed variations in channel gradient (Fig. 11a). Channel gradient approaches 1.47° (25.7 m/km) in the first interval, where the steepest parts of the channel are recorded (Fig. 11a). Between 12 km and 27 km in interval 2, the channel shows a stepped profile and gradient decreases to 0.83° (14.5 m/km) due to the presence of salt diapir D5. In the remainder of the channel (interval 3), channel gradient decreases to 0.71° (12.4 m/km) between 27 and 37 m, and reaches its lowest value of 0.5° (8.7 m/km) in the last 8 km (Fig. 11a).

The along-slope depth profile of the channel bank shows marked changes (Fig. 11a), which correlate with variations in the channel height profile (Fig. 11b). There are three intervals observed in the depth profile of channel bank and channel-height profile (Figs. 11a and b). The first interval (0-12 km) has the highest value of channel height, which ranges from 80 m to 156 m (Fig. 11b). In interval 2, between 12 and 27 km, the channel height decreases rapidly due to a decrease in the depth of the channel bank (Figs. 11a and b). The channel height reaches a minimum value of 13 m at 21 km, and then fluctuates between 22 m and 58 m for the remainder of interval 2 (Fig. 11b). The third interval starts with a marked increase in channel height from 22 m to 100 m at 27 km, due to an abrupt increase in the depth of the channel bank, and is followed by a decreasing trend. The channel height decreases to 26 m at the southern edge of the seismic volume (Fig. 11b).

6.1.2. Width profiles of channel and channel floor

The channel-width profile in Fig. 11c displays four intervals. It fluctuates between 445 and 1061 m in the first 13 km within interval 1. In interval 2, the channel width decreases from 689 m to its lowest value of 243 m at 27 km. This decreasing trend is followed by an increase of channel width between 27 km and 32 km (interval 3), where the channel width ranges from 403 m to 610 m. In interval 4, the channel width decreases rapidly to 310 m at 32 km and then rises progressively. It increases to 440 m at the southern limit of the seismic volume (Fig. 11c).

The width of the channel floor varies from 80 to 400 m, showing an average value of 203 m, and its profile can be divided in four intervals (Fig. 11c). For most of the channel length, channel-floor width shows small variations, but displays two increasing trends starting at 12 km in interval 2 and 36 km in interval 3 (Fig. 11c). These two trends relate to decreases in channel gradient at 12 km and 36 km (Figs. 11a and c).

6.1.3. Aspect ratio (width/height) and cross-sectional area (CSA) of channel

The aspect ratio of the channel ranges from 5 to 27 and four intervals are observed along the channel (Fig. 11d). It shows small changes in the first 13 km, with an average value of 6 in interval 1. The aspect ratio rises in interval 2, between 13 km and 21 km, and increases to a maximum of 27 at 21 km. The third interval starts with an abrupt drop at 21 km, where the aspect ratio decreases to 9 and then remains nearly constant. Between 27.5 and 36.5 km (interval 4), the aspect ratio displays an increasing trend towards the southern limit of the seismic volume, where the ratio increases up to 17 (Fig. 11d).

The CSA of the channel shows a similar trend to channel height and width (Figs. 11b, c and e). The CSA is ~ 0.06 km² in the first 10 km, except for an abrupt change at 2 km where the CSA decreases to 0.025 km² (Fig. 11e). Between 10 km and 25 km the CSA decreases by a factor of 22, from 0.067 km² at 10 km to a minimum value of 0.003 km² at 21 km. This significant reduction in CSA is followed by a nearly three-fold increase from 21 to 22 km, where it is 0.008 km² and remains constant for the next 3 km. The CSA shows a rapid increase from 25 km and an increase to 0.035

km² at 27 km. It then decreases gradually to 0.013 km² at 34 km, and varies between 0.009 km² and 0.02 km² for the remainder of the channel (Fig. 11e).

6.1.4. Variations in channel morphology

The channel displays significant morphological changes along the channel distance (Fig. 11 and Table 1). Five segments (Segments a to e) are observed following variations in channel morphological parameters (Figs. 10 and 11, Table 1).

In the first 13 km of Segment a, the channel is steepest and has the largest cross-section, as shown by the highest value of channel gradient, height, width and CSA (Fig. 11 and Table 1). In Segment b, between 13 km and 22 km, channel gradient decreases and is also accompanied by significant decreases of channel height, width and CSA (Fig. 11 and Table 1). For example, the channel width decreases more than 200 m and the CSA decreases by a factor of nearly 40 in this segment when compared to Segment a (Table 1). However, the width of the channel floor and the aspect ratio increase to their maxima value against reduced channel size in Segment b (Figs. 11b-e and Table 1).

In Segment c (22-27 km), the channel size decreases to its lowest value, with channel height of 38 m, channel-floor width of 165 m, channel width of 345 m and CSA of 0.008 km² (Table 1). The aspect ratio of the channel declines to 9 in this segment (Table 1).

In Segment d, abrupt increases in channel height and width are observed between 27 km and 32 km. These are accompanied by a nearly four-fold increase in the channel CSA when compared to Segment c (Figs. 11b, c and e, Table 1). In Segment e (32-42 km), channel width, height and CSA decrease again with increasing aspect ratios (Figs. 11b-e and Table 1).

6.2. Quantitative valley analyses

The valley is divided into three segments (Segments A to C) based on the observed changes in valley morphology (Figs. 10 and 12, Table 2). The valley shows multiple architectural elements (e.g. terraces and scars) in distinct segments (Fig. 10).

6.2.1. Depth profiles of valley thalweg and valley wall, and valley height profile

There are five intervals observed in the depth profile of the valley thalweg (Fig. 12a). The valley is steepest in the first 6 km, with a gradient of 1.88° (32.8 m/km). The valley gradient decreases to 1.34° (23.4 m/km) between 6 km and 13 km due to the presence of salt diapir D5. For the next 3 km, the valley thalweg is difficult to recognise because it presents similar seismic facies to an underlying MTD, both of which are composed of discontinuous, high amplitude reflections. Between 16 km and 22 km the valley gradient declines to 1.04° (18.2 m/km), and is then followed by an increase to 1.39° (24.3 m/km). In the remainder of the valley, the valley gradient decreases to its lowest value of 0.65° (11.3 m/km) between 30 m and 35 m (Fig. 12a).

The depth profile of the valley wall shows its steepest interval in the first 4 km, with a gradient of 2.01° (35.1 m/km) (Fig. 12a). This interval is followed by a decrease in valley-wall gradient to 1.28° (22.3 m/km) between 4 and 21 km, and 0.72° (12.6 m/km) from 21 to 27 km. In the fourth interval, between 27 and 35 km, the valley-wall gradient increases to 1.08° (18.9 m/km) (Fig. 12a).

The valley height is dependent on variations in both the depth of valley wall and valley thalweg (Figs. 12a and b). It ranges from 230 m to 350 m along the full length of the valley (Fig. 12b). In

interval 1, the valley height decreases due to a rapid drop in valley-wall depth (Figs. 12a and b). This trend is followed by an increase in valley height in the second interval (4-21 km), where it changes from 230 m to 310 m. The valley height decreases to its lowest value of 230 m at the end of interval 2. In interval 3, the valley height shows a marked increase. It increases to the highest value of 350 m at 29 km and is followed by a decrease in the remainder of the valley (Fig. 12b).

6.2.2. Width profiles of valley and valley base

The width profiles of the valley and the valley base share similar patterns. They both have relatively higher average values in interval 2 than those in intervals 1 and 3 (Fig. 12c).

The valley width ranges from 732 m to 2755 m (Fig. 12c). It fluctuates between 732 m and 1439 m in interval 1 (0-17 km). This fluctuation is followed by an increase to 2260 m between 17 m and 24 km in interval 2 (Fig. 12c). In interval 3 (24-35 km), valley width varies from 1000 m to 1500 m, with two maxima of 2187 m at 26.4 km and 2755 m at 33.25 km. The latter value of 2755 m represents where the valley width reaches its maximum (Fig. 12c).

The width of the valley base varies from 161 m to 700 m for most part of the valley. However, a rapid increase occurs between 19 km and 23 km, where the valley base can be up to 1738 m wide and an increase in valley width is also recorded (Fig. 12c).

6.2.3. Aspect ratio and cross-sectional area (CSA) of valley

The aspect ratio of the valley has a similar trend to the valley width (Figs. 12c and d), suggesting the valley width varies relatively more than the valley height. The aspect ratio ranges from 3 to 5 in the first 20 km. It is followed by an increase in interval 2 (20-24 km), where the aspect ratio rises up to 9. The aspect ratio decreases to 4 for the majority of interval 3 (24-35 m) but with two peak values, 7 at 26.5 m and 9 at 33.5 m, induced by the increased valley width (Fig. 12d).

The valley CSA also shares a similar pattern to valley width (Figs. 12c and e). The CSA is highest between 17 m and 23 m in interval 2, where it ranges from 0.253 km² to 0.431 km², whereas it varies between 0.087 and 0.337 km² in intervals 1 and 3 (Fig. 12e).

6.2.4. Variations in valley morphology

The valley is divided into three segments based on the observed morphological variations (Figs. 10 and 12, Table 2). These segments have similar aspect ratios but different valley sizes (Table 2).

The valley is smallest in Segment A, showing the lowest average value of valley-base width of 382 m, valley width of 1117 m, valley height of 273 m and CSA of 0.181 km² (Table 2). In Segment A, the terraces on the eastern wall of the valley are interpreted to result from the deposition of internal levees above slump deposits (Figs. 13a and b). Transparent to low amplitude, chaotic reflections are observed at the valley base (Figs. 13a and b). Similar seismic facies have been previously documented and interpreted as slump and debris-flow deposits sourced from the valley walls (Mayall et al., 2006; Gee et al., 2007; Janocko et al., 2013). These slump deposits are observed in the first 8 km of Segment A. The marked continuity of depositional patterns for such a long distance (8 km) suggests slumps were generated on the upper slope, and not locally on the valley walls.

In Segment B, between 17 and 24 km, the width of the valley base and the valley record maximum average values of 849 m and 1602 m, respectively (Table 2). This is particularly observed when considering the width of the valley base, which increases more than two-fold from Segment

A to Segment B (Table 2). Such an increase results in a relatively higher CSA value in Segment B (Table 2). The increase in valley size in Segment B is interpreted to result from cut bank erosion during lateral channel migration. Turbidity flows undercut the lower part of the valley and are followed by the collapse of overhanging blocks (i.e. cantilever failure), leading to the lateral widening of the valley, especially the valley base.

Discontinuous, high-amplitude seismic reflections at the valley base are interpreted as basal lags (Figs. 13c and d). Multiple channel forms are identified at the valley base and show the trajectory of lateral channel migrations (Figs. 13c and d) to be consistent with observations in Deptuck et al. (2003) and with models proposed by Sylvester et al. (2011). Moderate- to high-amplitude, parallel reflections are observed above basal lags (Figs. 13c and d). Similar reflections are also recorded by Deptuck et al. (2003), but it is difficult to identify them as abandoned channel-fills or overbank deposits (Deptuck et al., 2003, 2007). Some wedge-shaped seismic reflections can, however, be interpreted as internal levees of the channel system (Figs. 13c and d).

The architecture of the valley fill in this work is similar to that of Benin's and Niger delta's submarine channel systems (Deptuck et al., 2003). The presence of channel forms at the valley base suggest abrupt, and discrete lateral channel migration (Deptuck et al., 2007). Similar migration processes have also been recorded in the Lucia Chica channel system offshore California (Maier et al., 2012). This type of migration contrasts with the relatively continuous migration process revealed by Lateral Accretion Packages (LAPs) on seismic data from West Africa (Abreu et al., 2003; Janocko et al., 2013).

The size of the valley decreases in Segment C, as shown by relatively lower values of the valley width and the CSA when compared to Segment B, despite the fact that the largest valley height is observed in Segment C (Table 2). Arcuate scars of different sizes are observed on the banks of the channel belt in Segment C, some of them are located on the inner banks of the channel belt (Figs. 10 and 13e-g). These scars occur 70 m -140 m above the present-day channel thalweg, suggesting they were formed by shallow-seated mass failures (Figs. 13e-g). The presence of slide scars coincides spatially with the peak value in valley width at 26-27 km and 33-34 km (Figs. 10 and 12c), indicating that the valley was widened through shallow-seated mass failures in this segment. Terraces in this segment were formed by the deposition of internal levees (Figs. 13e and f) and failed blocks (Fig. 13g).

7. Discussion

7.1. Possible causes for variations in channel and valley morphology

In terms of hierarchical scheme, the seafloor channel in this study is comparable to channel elements from the stratigraphic record (Fig. 14). They are all considered as basic architectural elements of a stratal hierarchical framework.

The valley is the highest-order architectural element when considering the hierarchical (channel) framework described in this paper (Fig. 14). It is an integrated result of lateral migration and vertical stacking of channel elements through time, as shown by the shift of channel forms at the valley base (Figs. 13c-g). This observation is consistent with previous studies, which have shown that valley base is a diachronous surface or a composite erosional surface shaped by multiple erosional events (e.g. Deptuck et al., 2003; Sylvester et al., 2011; Kolla et al., 2012; Thomas and

Bodin, 2013; Macauley and Hubbard, 2013; Bain and Hubbard, 2016; Di Celma et al., 2011).

7.1.1. Channel morphology

The morphology of channel cross section shows significant variations along the channel (Fig. 11 and Table 1). This is shown, for example, by the rapid decrease in channel CSA from Segment a to Segment c, which decreases by a factor of 70 (Table 1).

Channel gradient is considered to be a major control on turbidity-flow behavior (e.g. Friedmann et al., 2000; Babonneau et al., 2002; McHargue et al., 2011; Wynn et al., 2012; Stevenson et al., 2013). Correlations between decreasing channel gradients and widened channel floors have been observed at 12 km and 36 km along the channel axis (Figs. 11a and c). These correlations are consistent with results from previous studies (Babonneau et al., 2002).

Apart from widened channel floors, decreases in channel gradient could also lead to reduced flow energy, sediment deposition, widened channels and decreased channel heights (e.g. Friedmann et al., 2000; Adeogba et al., 2005; Estrada et al., 2005). However, this is not strictly valid for the submarine channel investigated in this work. In our example, decreasing channel gradient from Segment a to Segments b and c is accompanied by decreased channel width (Table 1). A similar relationship is also observed from Segment d to Segment e (Table 1). Additionally, increased channel height with decreased channel gradient from Segment c to Segment d also contradicts previous work. Therefore, channel gradient probably is not the main cause for the variations in channel size documented here.

Because the height of the leveed channel indicates the minimum thickness of turbidity-flows that forming internal levees, and can thus be used as an indicator of flow volume (Babonneau et al., 2002; Deptuck et al., 2003; Estrada et al., 2005), spatial variations in channel height along the channel length suggest that flows inside the channel were not the same in terms of their physical properties and erosional power. Such variations may reveal spatial and temporal variations in flow volume. This observation agrees with the models proposed in McHargue et al. (2011), who suggests multiple waxing-waning cycles of turbidity flows at multiple scales.

Relationships between temporal changes in flow properties and channel size have been observed in the Niger delta, where a temporal decrease in channel size is correlated with a decrease in sediment supply (Jobe et al., 2015). Similar scenarios may also occur in the studied channel. The volume of turbidity flows flushed into the channel may have decreased through time, leading to smaller channels in Segments b, c d, and e. Additionally, tributaries in the confluence region could have induced variations in channel size. Apart from the intersection of the west tributary with the main seafloor channel observed at the confluence point, two other tributary channels connecting to the east tributary are observed on the seafloor (Fig. 9). These tributaries may have provided low-volume, and less energetic flows to the main pathway. These flows tended to deposit in Segments b and c, rather than transporting sediments downslope towards Segments d and e, therefore generating small-sized channels in Segments b and c.

Despite the observed variations in channel size, the width of the channel floor shows relatively small changes (Fig. 11c and Table 1), suggesting it has been only slightly affected by variations in flow discharge.

7.1.2. Valley morphology

Valley morphology reveals spatial variations in erosional processes within the valley. It is

difficult to identify the principal erosional mechanism in Segment A, but the morphology and architecture of the valley suggest spatial variations in erosional processes in both Segments B and C.

In Segment B, the valley base is more than two times wider than other segments (Table 2). This difference is interpreted as resulting from cut bank erosion during multiple episodes of lateral channel migration (Fig. 15a), as shown by the channel forms at the valley base (Figs. 13c and d). Cantilever failure probably is the main erosional processes in this segment.

In Segment C, inner bank erosion in the form of shallow-seated mass failures (Figs. 13e-g) widened the upper part of the valley wall, and resulted in a stepped bank profile (Fig. 15b). Similar mass failures and associated scars have also been recorded in other submarine channels (e.g. Deptuck et al., 2007; Janocko et al., 2013), they are contrast with deep-seated mass failures observed in the submarine channel system of the Gulf of Mexico (Sawyer et al., 2013). In addition, shallow-seated mass failures are mainly located in Segment C (Fig. 10), suggesting local factors predominantly control bank erosion in this area. A marked increase in valley height from Segment B to Segment C reflects this process, as the increase may be associated with the occurrence of scars and associated mass wasting in Segment C (Fig. 12b).

Spatial variations in valley morphology suggest valley size can change over a short distance (i.e. a few kilometers), as documented by the two-fold increase in valley CSA in Segment B, within just 7 km (Table 2). Such an increase in valley size can enhance the volume of channel-fill deposits and the reservoir potential of the valley, but the extent of valley enlargement is relatively small, increasing uncertainty when drilling.

7.2. Scale comparison with other submarine channel systems

This work shows a channel of 243-1061 m wide, and 13-156 m high (Figs. 11b and c). Channels hundreds of meters wide, tens of meters high have been documented, on seismic data in the Gulf of Mexico (Sylvester et al., 2012) and Congo (Deptuck et al., 2007; Jobe et al., 2015), and on bathymetric data from offshore California (Maier et al., 2012). Similar channels have also been documented at outcrops (Brunt et al., 2013; Figueiredo et al., 2013; Gardner et al., 2003; Di Celma et al., 2011; Moody et al., 2012; Bain and Hubbard, 2016). Furthermore, km-wide channels are recorded in the modern Amazon and Zaire fans (Pirmez and Flood, 1995; Babonneau et al., 2002). As submarine channels are products of turbidity flows, changes in their size probably reflect variations in flow properties (e.g. flow volume, grain-size distribution) (e.g. Babonneau et al., 2002; Pirmez and Imran, 2003; Sequeiros, 2012; Konsoer et al., 2013; Jobe et al., 2015).

The valley is 700-2800 m wide, 230-350 m high in this study (Figs. 12b and c). Similar valleys have been documented from both seismic (e.g. Wood and Mize-spansky, 2009; Gamberi et al., 2013) and outcrop studies (e.g. Masalimova et al., 2016). However, valleys (or channel complexes) documented in the literature show marked variations in their height and width. For example, channel complexes less than 1000 m wide have been recorded at outcrop in North America (Pyles et al., 2010; Gardner et al., 2003), Italy (Thomas and Bodin, 2013) and Chile (Macauley and Hubbard, 2013). In contrast, valleys more than 3000 m wide have been recorded on seismic data (e.g. Samuel et al., 2003; Deptuck et al., 2007; Catteral et al., 2010; De Ruig and Hubbard, 2006; Kolla et al., 2012; Jolly et al., 2016), and at outcrops (e.g. Bain and Hubbard, 2016; Grecula et al., 2003). In the Indus fan, the valley can be up to 10 km wide (Deptuck et al., 2003). These marked variations may

relate to the degree of lateral channel migration. This seems to be the case for the studied submarine channel, where the higher degree of lateral migration corresponds to the largest valley width and CSA in Segment B (Figs. 13c and d, Table 2). In contrast, the lower degree of lateral migration resulted in lower valley width and CSA (Figs. 13e-g, Table 2). Spatial correlation between channel Segments b and c, and valley Segment B (Fig. 10) suggests that increased degree of lateral channel migration in Segment B may be associated with local sediment input from tributaries. Apart from cut bank erosion during lateral channel migration, inner bank erosion has also contributed to the widening of the valley, as reflected by the shallow-seated mass failures and associated scars observed in this study (Figs. 10 and 13e-g).

The distinct channel and valley scale-relationships obtained from previous studies are also dependent on the data sources utilised and on the measurement methods applied (Kolla et al., 2001; Wood and Mize-spansky, 2009; McHargue et al., 2011). Because of data resolution, seismic data seldom reveal small-scale channels, which may be only a single wavelength thick. Measurements performed on planform and cross-sections can make a difference to morphometric analyses (e.g. Wood and Mize-spansky, 2009). Channel and valley width may be overestimated when outcrops are not perpendicular to the channel and valley axis, whereas they may be underestimated because muddy deposits at the top of channel fill tend to be eroded and poorly exposed (McHargue et al., 2011).

8. Conclusions

This study focuses on the geomorphology and bank erosional processes of a late Pleistocene-Holocene channel system developed in the Espírito Santo Basin, SE Brazil, to conclude:

a) On channel scale of a fundamental hierarchical level, five segments (Segments a to e) are identified based on the variations in morphologic parameters. The observed variations are related to spatial and temporal changes of flow volume within the channel.

b) On valley scale of a higher-order hierarchical level, three segments (Segments A to C) are recognised according to the morphological changes of the valley. The variations of valley morphology was controlled by two distinct erosional processes. Cut bank erosion during lateral channel migration led to the retreat of entire valley walls, especially widening the valley base in Segment B. In contrast, inner bank erosion in the form of shallow-seated mass failures only enlarged the upper part of the valley wall, as in Segment C.

c) The scales of channel and valley in this study are comparable to examples observed on other continental slopes. Distinct spatial variations in both channel and valley morphology in the same channel system suggest an important role of local factors (e.g. salt diapirs, tributaries, overbank collapse) on its development and later evolution.

d) Relative increases in valley size are capable to enhance the volume of channel-fill deposits, but the extent of valley enlargement is relatively small in this study. In terms of reservoir potential, one should take into account the combined nature (i.e., net-to-gross ratios) and volume of levee and adjacent channel-fill deposits.

Acknowledgements

The authors thank CGG for the permission to use the 3D seismic data in this article. Stephen

Hubbard and an anonymous reviewer are acknowledged for their constructive comments, which have significantly improved the article. Davide Gamboa publishes with the permission of the Executive Director, British Geological Survey.

References

- Antobreh, A.A., Krastel, S., 2006. Morphology, seismic characteristics and development of Cap Timiris Canyon, offshore Mauritania: a newly discovered canyon preserved off a major arid climatic region. *Mar. Pet. Geol.* 23, 37-59.
- Abreu, V., Sullivan, M., Pirmez, C., Mohrig, D., 2003. Lateral accretion packages (LAPs): an important reservoir element in deep water sinuous channels. *Mar. Pet. Geol.* 20, 631-648.
- Adeogba, A.A., McHargue, T.R., Graham, S.A., 2005. Transient fan architecture and depositional controls from near-surface 3-D seismic data, Niger Delta continental slope. *Am. Assoc. Pet. Geol. Bull.* 89, 627-643.
- Alves, T.M., Cartwright, J., Davies, R.J., 2009. Faulting of salt-withdrawal basins during early halokinesis: effects on the Paleogene Rio Doce canyon system (Espírito Santo basin, Brazil). *Am. Assoc. Pet. Geol. Bull.* 93, 617-652.
- Alves, T.M., 2012. Scale-relationships and geometry of normal faults reactivated during gravitational gliding of Albian rafts (Espírito Santo Basin, SE Brazil). *Earth Planet. Sci. Lett.* 331-332, 80-96.
- Bain, H.A., Hubbard, S.M., 2016. Stratigraphic evolution of a long-lived submarine channel system in the late cretaceous nanaimo group, British Columbia, Canada. *Sediment. Geol.* 337, 113-132.
- Babonneau, N., Savoye, B., Cremer, M., Klein, B., 2002. Morphology and architecture of the present canyon and channel system of the Zaire deep-sea fan. *Mar. Pet. Geol.* 19, 445-467.
- Babonneau, N., Savoye, B., Cremer, M., Bez, M., 2004. Multiple terraces within the deep incised Zaire Valley (ZaiAngo Project): are they confined levees? *Geol. Soc. Lond. Spec. Publ.* 222, 91-114.
- Bastos, C., Quaresma, V., Marangoni, M., D'Agostini, D., Bourguignon, S., Cetto, P., Silva, A., Filho, G., Moura, R., Collins, M., 2015. Shelf morphology as an indicator of sedimentary regimes: a synthesis from a mixed siliciclastic-carbonate shelf on the eastern Brazilian margin. *J. S. Am. Earth Sci.* 63, 125-136.
- Baudon, C., Cartwright, J., 2008. The kinematics of reactivation of normal faults using high resolution throw mapping. *J. Struct. Geol.* 30, 1072-1084.
- Bruhn, C.H.L., Walker, R.G., 1997. Internal architecture and sedimentary evolution of coarse-grained, turbidite channel-levee complexes, early Eocene Regência canyon, Espírito Santo Basin, Brazil. *Sedimentology* 44, 17-46.
- Brunt, R., Di Celma, C., Hodgson, D., Flint, S., Kavanagh, J., Van der Merwe, W., 2013. Driving a channel through a levee when the levee is high: an outcrop example of submarine down-dip entrenchment. *Mar. Pet. Geol.* 41, 134-145.
- Campion, K.M., Sprague, A.R., Mohrig, D., Lovell, R.W., Drzewiecki, P.A., Sullivan, M.D., Ardill, J.A., Jensen, G.N., Sickafoose, D.K., 2000. Outcrop expression of confined channel complexes. In: Weimer, P., Slatt, R.M., Coleman, J., Rosen, N.C., Nelson, H., Bouma, A.H., Styzen, M.J., Lawrence, D.T. (Eds.), *Deepwater Reservoirs of the World*. Gulf Coast Section SEPM 20th

- Bob F. Perkins Research Conference, pp. 127-150.
- Catterall, V., Redfern, J., Gawthorpe, R., Hansen, D., Thomas, M., 2010. Architectural style and quantification of a submarine channel-levee system located in a structurally complex area: offshore Nile Delta. *J. Sediment. Res.* 80, 991-1017.
- Chang, H.K., Kowsmann, R.O., Figueiredo, A.M., Bender, A.A., 1992. Tectonics and stratigraphy of the East Brazil Rift system-an overview. *Tectonophysics* 213, 97-138.
- Clark, J.D., Kenyon, N.H., Pickering, K.T., 1992. Quantitative analysis of the geometry of submarine channels: implications for the classification of submarine fans. *Geology* 20, 633-636.
- Clark, I.R., Cartwright, J.A., 2009. Interactions between submarine channel systems and deformation in deep-water fold belts: examples from the Levant Basin, Eastern Mediterranean Sea. *Mar. Pet. Geol.* 26, 1465-1482.
- Cobbold, P.R., Meisling, K.E., Mount, V.S., 2001. Reactivation of an obliquely rifted margin, Campos and Santos basins, southeastern Brazil. *Am. Assoc. Pet. Geol. Bull.* 85, 1925-1944.
- Cordani, U.G., 1970. Idade do vulcanismo no Oceano Atlântico Sul, vol. 1. *Boletim do Instituto de Geociências e Astronomia da Universidade de São Paulo*, pp. 9 ~ 76.
- Davison, I., 1999. Tectonics and hydrocarbon distribution along the Brazilian south Atlantic margin. In: Cameron, N.R., Bate, R.H., Clure, V.S. (Eds.), *The Oil and Gas Habitats of the South Atlantic*, vol. 153. Geological Society London Special Publications, pp. 133-151.
- Demercian, S., Szatmari, P., Cobbold, P.R., 1993. Style and pattern of salt diapirs due to thin-skinned gravitational gliding, Campos and Santos basins, offshore Brazil. *Tectonophysics* 228, 393-433.
- Deptuck, M.E., Steffens, G.S., Barton, M., Pirmez, C., 2003. Architecture and evolution of upper fan channel-belts on the Niger Delta slope and in the Arabian Sea. *Mar. Pet. Geol.* 20, 649-676.
- Deptuck, M.E., Sylvester, Z., Pirmez, C., O'Byrne, C., 2007. Migration-aggradation history and 3-D seismic geomorphology of submarine channels in the Pleistocene Benin-major Canyon, western Niger Delta slope. *Mar. Pet. Geol.* 24, 406-433.
- De Ruig, M.J., Hubbard, S.M., 2006. Seismic facies and reservoir characteristics of a deep-marine channel belt in the Molasse foreland basin, Puchkirchen Formation, Austria. *Am. Assoc. Pet. Geol. Bull.* 90, 735-752.
- Di Celma, C.N., Brunt, R.L., Hodgson, D.M., Flint, S.S., Kavanagh, J.P., 2011. Spatial and temporal evolution of a Permian submarine slope channel-levee system, Karoo Basin, South Africa. *J. Sediment. Res.* 81, 579-599.
- Dominguez, J.M.L., Bittencourt, A.C.S.P., Martin, L., 1992. Controls on Quaternary coastal evolution of the east-northeastern coast of Brazil: roles of sea-level history, trade winds and climate. *Sediment. Geol.* 80, 213-232.
- Estrada, F., Ercilla, G., Alonso, B., 2005. Quantitative study of a Magdalena submarine channel (Caribbean Sea): implications for sedimentary dynamics. *Mar. Pet. Geol.* 22, 623-635.
- Fiduk, J.C., Brush, E.R., Anderson, L.E., Gibbs, P.B., Rowan, M.G., 2004. Salt deformation, magmatism, and hydrocarbon prospectivity in the Espírito Santo Basin, offshore Brazil. In: Post, P.J., et al. (Eds.), *Salt-sediment Interactions and Hydrocarbon Prospectivity: Concepts, Applications, and Case Studies for the 21st Century*. GCSSEPM 24th Annual Research Conference, pp. 370-392.
- Figueiredo, J.J.P., Hodgson, D.M., Flint, S.S., Kavanagh, J.P., 2013. Architecture of a channel

- complex formed and filled during long-term degradation and entrenchment on the upper submarine slope, Unit F, Fort Brown Fm., SW Karoo Basin, South Africa. *Mar. Pet. Geol.* 41, 104-116.
- Flood, R.D., Damuth, J.E., 1987. Quantitative characteristics of sinuous distributary channels on the Amazon deep-sea fan. *Geol. Soc. Am. Bull.* 98, 728-738.
- França, R.L., Del Rey, A.C., Tagliari, C.V., Brandão, J.R., De Rossi Fontanelli, P., 2007. Bacia Do Espírito Santo, vol. 15. *Boletim de Geociências da Petrobras*, pp. 501-509.
- Friedmann, S.J., Beaubouef, R.T., Pirmez, C., Jennette, D.C., 2000. The effects of gradient changes on deep-water depositional systems: an integrated approach. In: American Association of Petroleum Geologists, 2000 Annual Meeting, Extended Abstracts, New Orleans, U.S, p. 51.
- Gamboa, D., Alves, T.M., 2015. Spatial and dimensional relationships of submarine slope architectural elements: a seismic-scale analysis from the Espírito Santo Basin (SE Brazil). *Mar. Pet. Geol.* 64, 43-57.
- Gamboa, D., Alves, T.M., Cartwright, J., 2012. A submarine channel confluence classification for topographically confined slopes. *Mar. Pet. Geol.* 35, 176-189.
- Gamberi, F., Rovere, M., Dykstra, M., Kane, I.A., Kneller, B.C., 2013. Integrating modern seafloor and outcrop data in the analysis of slope channel architecture and fill. *Mar. Pet. Geol.* 41, 83-103.
- Gamboa, D., Alves, T., Cartwright, J., Terrinha, P., 2010. MTD distribution on a 'passive' continental margin: the Espírito Santo Basin (SE Brazil) during the Paleogene. *Mar. Pet. Geol.* 7, 1311-1324.
- Gardner, M.H., Borer, J.M., 2000. Submarine channel architecture along a slope to basin profile, Brushy Canyon Formation, West Texas. In: Bouma, A.H., Stone, C.G. (Eds.), *Fine-grained Turbidite Systems. Memoir 72-American Association of Petroleum Geologists and Special Publication 68-SEPM*, pp. 195-214.
- Gardner, M.H., Borer, J.M., Melik, J.J., Mavilla, N., Dechesne, M., Wagerle, R.D., 2003. Stratigraphic process-response model for submarine channels and related features from studies of Permian Brushy Canyon outcrops, West Texas. *Mar. Pet. Geol.* 20, 757-788.
- Gee, M.J.R., Gawthorpe, R.L., Bakke, K., Friedmann, S.J., 2007. Seismic geomorphology and evolution of submarine channels from the Angolan continental margin. *J. Sediment. Res.* 77, 433-446.
- Georgiopoulou, A., Cartwright, J.A., 2013. A critical test of the concept of submarine equilibrium profile. *Mar. Pet. Geol.* 41, 35-47.
- Grecula, M., Flint, S.S., Wickens, H.D., Johnson, S.D., 2003. Upward-thickening patterns and lateral continuity of Permian sand-rich turbidite channel fills, Laingsburge Karoo, South Africa. *Sedimentology* 50, 831-853.
- Hansen, L.A.S., Callow, R.H.T., Kane, I.A., Gamberi, F., Rovere, M., Cronin, B.T., Kneller, B.C., 2015. Genesis and character of thin-bedded turbidites associated with submarine channels. *Mar. Pet. Geol.* 67, 852-879.
- Hubbard, S.M., Covault, J.A., Fildani, A., Romans, B.R., 2014. Sediment transfer and deposition in slope channels: deciphering the record of enigmatic deep-sea processes from outcrop. *Geol. Soc. Am. Bull.* 126, 857-871.
- Hubbard, S.M., De Ruig, M.J., Graham, S.M., 2009. Confined channel-levee complex development in an elongate depocenter: deep-water Tertiary strata of the Austrian Molasse Basin. *Mar. Pet.*

- Geol. 26, 85-112.
- Hubbard, S.M., Romans, B.W., Graham, S.A., 2008. Deep-water foreland basin deposits of the Cerro Toro Formation, Magallanes basin, Chile: architectural elements of a sinuous basin axial channel belt. *Sedimentology* 55, 1333-1359.
- Janocko, M., Nemeč, W., Henriksen, S., Warchoł, M., 2013. The diversity of deep-water sinuous channel belts and slope valley-fill complexes. *Mar. Pet. Geol.* 41, 7-34.
- Jobe, Z.R., Sylevster, Z., Parker, A.O., Howes, N., Slowey, N., Pirmez, C., 2015. Rapid adjustment of submarine channel architecture to changes in sediment supply. *J. Sediment. Res.* 85, 729-753.
- Jolly, B.A., Lonergan, L., Whittaker, A.C., 2016. Growth history of fault-related folds and interaction with seabed channels in the toe-thrust region of the deep-water Niger delta. *Mar. Pet. Geol.* 70, 58-76.
- Kane, I., Hodgson, D., 2011. Sedimentological criteria to differentiate submarine channel levee subenvironments: exhumed examples from the Rosario Fm. (Upper cretaceous) of Baja California, Mexico, and the Fort Brown Fm. (Permian), Karoo Basin, S. Africa. *Mar. Pet. Geol.* 28, 807-823.
- Kolla, V., Bourges, P., Urrity, J.M., Safa, P., 2001. Evolution of deep-water tertiary sinuous channels offshore, Angola (West Africa) and implications to reservoir architecture. *Am. Assoc. Pet. Geol. Bull.* 85, 1373-1405.
- Kolla, V., 2007. A review of sinuous channel avulsion patterns in some major deep-sea fans and factors controlling them. *Mar. Pet. Geol.* 24, 450-469.
- Kolla, V., Bandyopadhyay, A., Gupta, P., Mukherjee, B., Ramana, D.V., 2012. Morphology and internal structure of a recent upper Bengal Fan-Valley Complex. In: Prather, B.E., Deptuck, M.E., Mohrig, D., Van Hoorn, B., Wynn, R.B. (Eds.), *Application of the Principles Seismic Geomorphology to Continental Slope and Base-of-slope Systems: Case Studies from Seafloor and Near-seafloor*, vol. 99, pp. 347-369. SEPM Special Publication No.
- Knoppers, B., Ekau, W., Figueiredo, A.G., 1999. The coast and shelf of east and northeast Brazil and material transport. *Geo-Mar. Lett.* 19, 171-178.
- Konsoer, K., Zinger, J., Parker, G., 2013. Bankfull hydraulic geometry of submarine channels created by turbidity currents: relations between bankfull channel characteristics and formative flow discharge. *J. Geophys. Res. Earth Surf.* 118, 216-228.
- Lien, T., Walker, R.G., Martinsen, O.J., 2003. Turbidites in the Upper carboniferous Ross Formation, western Ireland: reconstruction of a channel and spillover system. *Sedimentology* 50, 113-148.
- Macauley, R.V., Hubbard, S.M., 2013. Slope channel sedimentary processes and stratigraphic stacking, Cretaceous Tres Pasos Formation slope system, Chilean Patagonia. *Mar. Pet. Geol.* 41, 146-162.
- Maier, K.L., Fildani, A., McHargue, T.R., Paull, C.K., Graham, S.A., Caress, D.W., 2012. Punctuated deep-water channel migration: high-resolution subsurface data from the Lucia Chica channel system, offshore California, USA. *J. Sediment. Res.* 82, 1-8.
- Martin, L., Suguio, K., 1992. Variation of coastal dynamics during the last 7000 years recorded in beach-ridge plains associated with river mouths: example from the central Brazilian coast. *Palaeogeogr. Palaeoclimatol. Palaeoecol.* 99, 119-140.
- Masalimova, L.U., Lowe, D.R., Sharman, G.R., King, P.R., Arnot, M.J., 2016. Outcrop characterization of a submarine channel-lobe complex: the lower mount messenger formation,

- Taranaki basin, New Zealand. *Mar. Pet. Geol.* 71, 360-390.
- Mayall, M., Jones, E., Casey, M., 2006. Turbidite channel reservoirs-Key elements in facies prediction and effective development. *Mar. Pet. Geol.* 23, 821-841.
- Mayall, M., Stewart, I., 2000. The architecture of turbidite slope channels. In: Weimer, P., Slatt, R.M., Coleman, J.L., Rosen, N., Nelson, C.H., Bouma, A.H., Styzen, M., Lawrence, D.T (Eds.), *Global Deep-water Reservoirs: Gulf Coast Section SEPM Foundation 20th Annual Bob F Perkins Research Conference*, pp. 578-586.
- McHargue, T., Pyrez, M.J., Sullivan, M.D., Clark, J.D., Fildani, A., Romans, B.W., Covault, J.A., Levy, M., Posamentier, H.W., Drinkwater, N.J., 2011. Architecture of turbidite channel systems on the continental slope: patterns and predictions. *Mar. Pet. Geol.* 28, 728-743.
- Mohriak, W.U., 2003. Bacias sedimentares da margem continental Brasileira. In: Bizzi, L.A., Schobbenhaus, C., Vidotti, R.M., Goncalves, J.H. (Eds.), *Geologia, Tectonica e Recursos Minerais do Brasil*. CPRM, Brasilia, pp. 87-165.
- Mohriak, W.U., Nemcok, M., Enciso, G., 2008. South Atlantic divergen margin evolution: rift-borded uplift and salt tectonics in the basins of Southeastern Brazil. In: Pankhurst, R.J., Trouw, R.A.J., Brito Neves, B.B., de Wit, M.J. (Eds.), *West Gondwana Pre-cenozoic Correlations across the South Atlantic Region*, Geological Society London, vol. 294, pp. 365-398. Special Publication.
- Moody, J.D., Pyles, D.R., Clark, J., Bouroullec, R., 2012. Quantitative outcrop characterization of an analog to weakly confined submarine channel systems: Morillo 1 member, Ainsa Basin, Spain. *Am. Assoc. Pet. Geol. Bull.* 96, 1813-1841.
- Ojeda, H.A.O., 1982. Structural framework, stratigraphy, and evolution of Brazilian marginal basins. *Am. Assoc. Pet. Geol. Bull.* 66, 732-749.
- Peakall, J., Kane, I.A., Masson, D.G., Keevil, G., McCaffrey, W.D., Corney, R., 2012. Global (latitudinal) variation in submarine channel sinuosity. *Geology* 40, 11-14.
- Pirmez, C., Flood, R.D., 1995. Morphology and structure of Amazon channel. In: Flood, R.D., Piper, D.J.W., Klaus, A., et al. (Eds.), *Proceedings of the Ocean Drilling Program*, vol. 155. TX (Ocean Drilling Program), College Station, pp. 23-45. Initial Reports.
- Pirmez, C., Imran, J., 2003. Reconstruction of turbidity currents in Amazon channel. *Mar. Pet. Geol.* 20, 823-849.
- Posamentier, H., 2003. Depositional elements associated with a basin floor channellevee system: case study from the Gulf of Mexico. *Mar. Pet. Geol.* 20, 677-690.
- Pyles, D.R., Jennette, D.C., Tomasso, M., Beaubouef, R.T., Rossen, C., 2010. Concepts learned from a 3D outcrop of a sinuous slope channel complex: Beacon Channel complex, Brushy Canyon Formation, West Texas, U.S.A. *J. Sediment. Res.* 80, 67-96.
- Samuel, A., Kneller, B., Raslan, S., Sharp, A., Parsons, C., 2003. Prolific deep-marine slope channels of the Nile Delta, Egypt. *Am. Assoc. Pet. Geol. Bull.* 87, 541-560.
- Sawyer, D.E., Flemings, P.B., Nikolinakou, M., 2013. Continuous deep-seated slope failure recycles sediments and limits levee height in submarine channels. *Geology* 42, 15-18.
- Sequeiros, O.A., 2012. Estimating turbidity current conditions from channel morphology: a Froude number approach. *J. Geophys. Res.* 117, C04003. <http://dx.doi.org/10.1029/2011JC007201>.
- Sprague, A.R., Sullivan, M.D., Champion, K.M., Jensen, G.N., Goulding, D.K., Sickafoose, D.K., Jennette, D.C., 2002. The physical stratigraphy of deep-water strata: a hierarchical approach to the analysis of genetically related elements for improved reservoir prediction. In: *American Association of Petroleum Geologists Annual Meeting Abstracts*, Houston, Texas, pp. 10-13.

- Sprague, A.R.G., Garfield, T.R., Goulding, F.J., Beaubouef, R.T., Sullivan, M.D., Rossen, C., Champion, K.M., Sickafoose, D.K., Abreu, V., Schellpeper, M.E., Jensen, G.N., Jennette, D.C., Pirmez, C., Dixon, B.T., Ying, D., Ardill, J., Mohrig, D.C., Porter, M.L., Farrell, M.E., Mellere, D., 2005. Integrated slope channel depositional models: the key to successful prediction of reservoir presence and quality in offshore West Africa. In: CIPM, Cuarto E-exitep 2005, February 20-23, 2005, Veracruz, Mexico, pp. 1-13.
- Stevenson, C.J., Talling, P.J., Wynn, R.B., Masson, D.G., Hunt, J.E., Frenz, M., Akhmetzhanov, A., Cronin, B.T., 2013. The flows that left no trace: very large volume turbidity currents that bypassed sediment through submarine channels without eroding the seafloor. *Mar. Pet. Geol.* 41, 186-205.
- Sylvester, Z., Pirmez, C., Cantelli, A., 2011. A model of submarine channel-levee evolution based on channel trajectories: implications for stratigraphic architecture. *Mar. Pet. Geol.* 28, 716-727.
- Sylvester, Z., Deptuck, M.E., Prather, B.E., Pirmez, C., O'Byrne, C., 2012. Seismic stratigraphy of a shelf-edge delta and linked submarine channels in the North-Eastern Gulf of Mexico. In: Prather, B.E., Deptuck, M.E., Mohrig, D., van Hoorn, B., Wynn, R. (Eds.), *Application of the Principles of Seismic Geomorphology to Continental-Slope and Base-of-slope Systems: Case Studies from Seafloor and Near-seafloor Analogues*, vol. 99, pp. 31-59. SEPM, Special Publication.
- Thomas, M., Bodin, S., 2013. Architecture and evolution of the Finale channel system, the Numidian Flysch formation of Sicily: insights from a hierarchical approach. *Mar. Pet. Geol.* 41, 163-185.
- Vigorito, M., Murru, M., Simone, L., 2006. Architectural patterns in a multistorey mixed carbonate-siliciclastic submarine channel, Porto Torres Basin, Miocene, Sardinia, Italy. *Sediment. Geol.* 186, 213-236.
- Wonham, J.B., Jayr, S., Mougamba, R., Chuilon, P., 2000. 3D sedimentary evolution of a canyon fill (lower Miocene-age) from the Mandorove Formation, offshore Gabon. In: Stow, V.D.A., Mayall, M. (Eds.), *Deep-water Sedimentary Systems: New Models for the 21st Century*. Pergamon, Oxford, pp. 175-197.
- Wood, L.J., Mize-spansky, K.L., 2009. Quantitative seismic geomorphology of a Quaternary leveed-channel system, offshore eastern Trinidad and Tobago, northeastern South America. *Am. Assoc. Pet. Geol. Bull.* 93, 101-125.
- Wynn, R.B., Cronin, B.T., Peakall, J., 2007. Sinuous deep-water channels: genesis, geometry and architecture. *Mar. Pet. Geol.* 24, 341-387.
- Wynn, R.B., Talling, P.J., Masson, D.G., Le Bas, T.P., Cronin, B.T., Stevenson, C.J., 2012. The Influence of Subtle Gradient Changes on Deep-water Gravity Flows: a Case Study from the Moroccan Turbidite System, vol. 99, pp. 371-383. SEPM Special Publication.

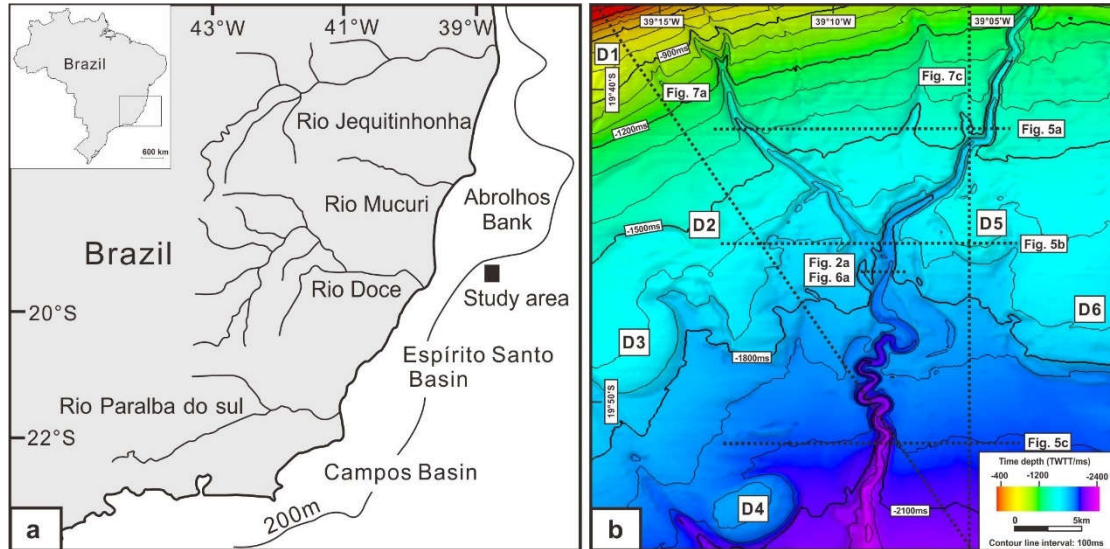


Fig. 1. (a) Regional map of the SE Brazilian Margin showing the location of the studied 3D seismic volume from the Espírito Santo Basin. (b) Contoured seafloor map of the study area generated from the interpreted seismic volume. It highlights the location of the modern channel relatively to salt diapirs D1 to D6.

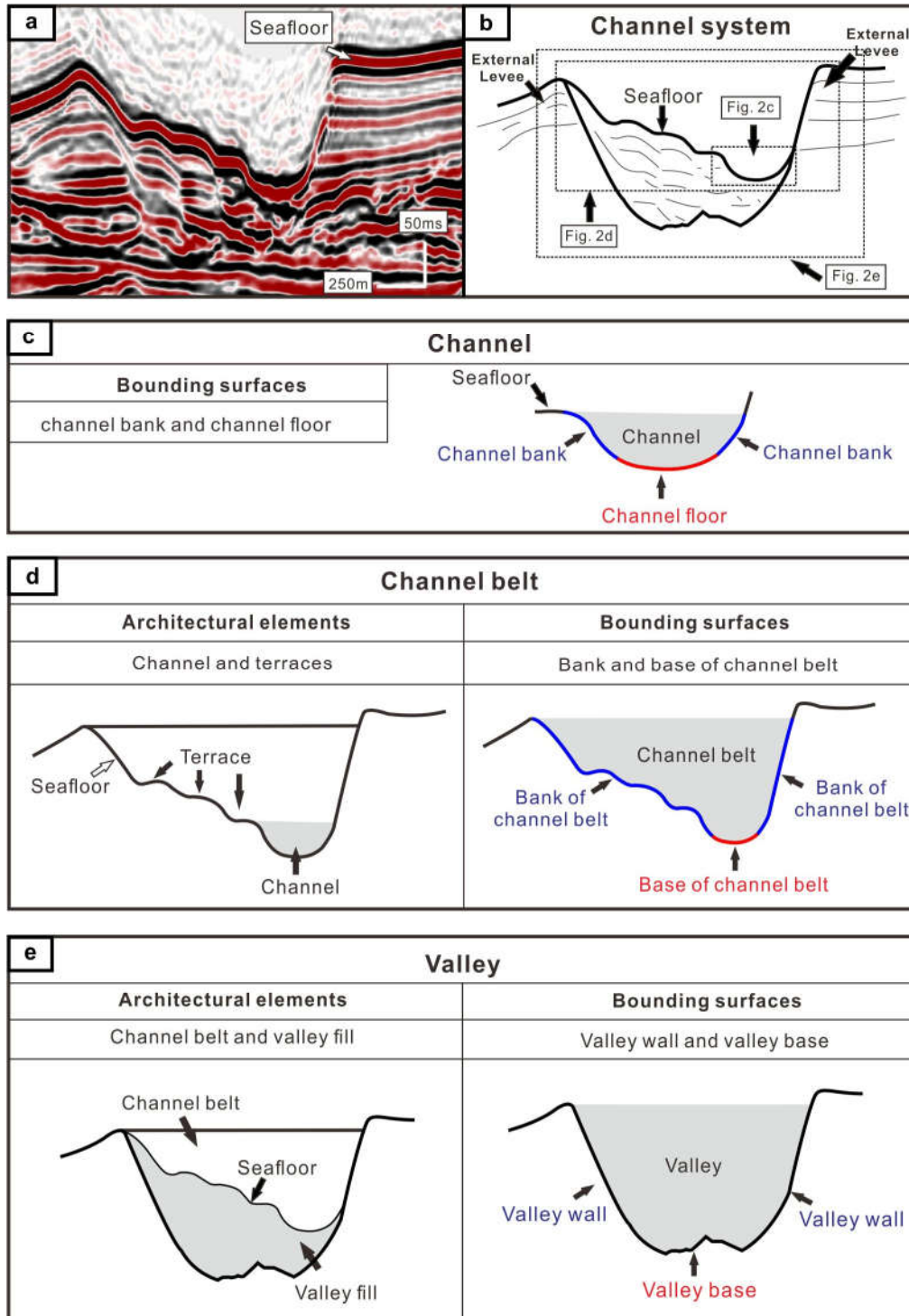


Fig. 2. Schematic diagrams summarising the terminology used in this study. (a) and (b) are uninterpreted and interpreted seismic sections showing the architecture of submarine channel systems in the study area. (c) Channel is defined as a V- or U-shaped negative relief on the seafloor. (b) Channel belt is a negative relief on the seafloor, and comprises channel and associated terraces. (d) Valley comprises a channel belt and valley fill. It is formed by a combination of lateral channel migration and the vertical aggradation of sediments.

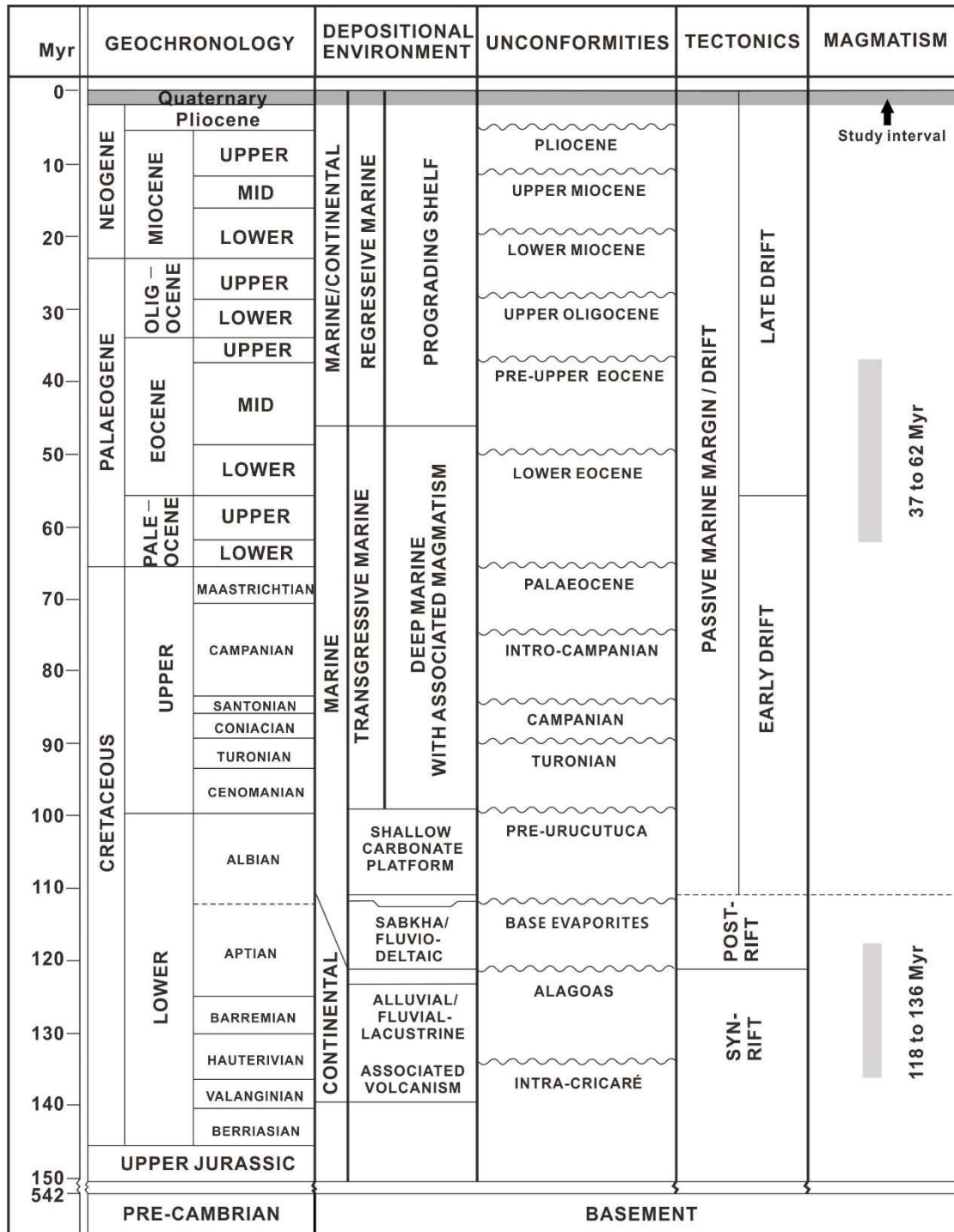


Fig. 3. Stratigraphic column of the Espírito Santo Basin showing main tectono-sedimentary stages and magmatic events (modified from França et al., 2007).

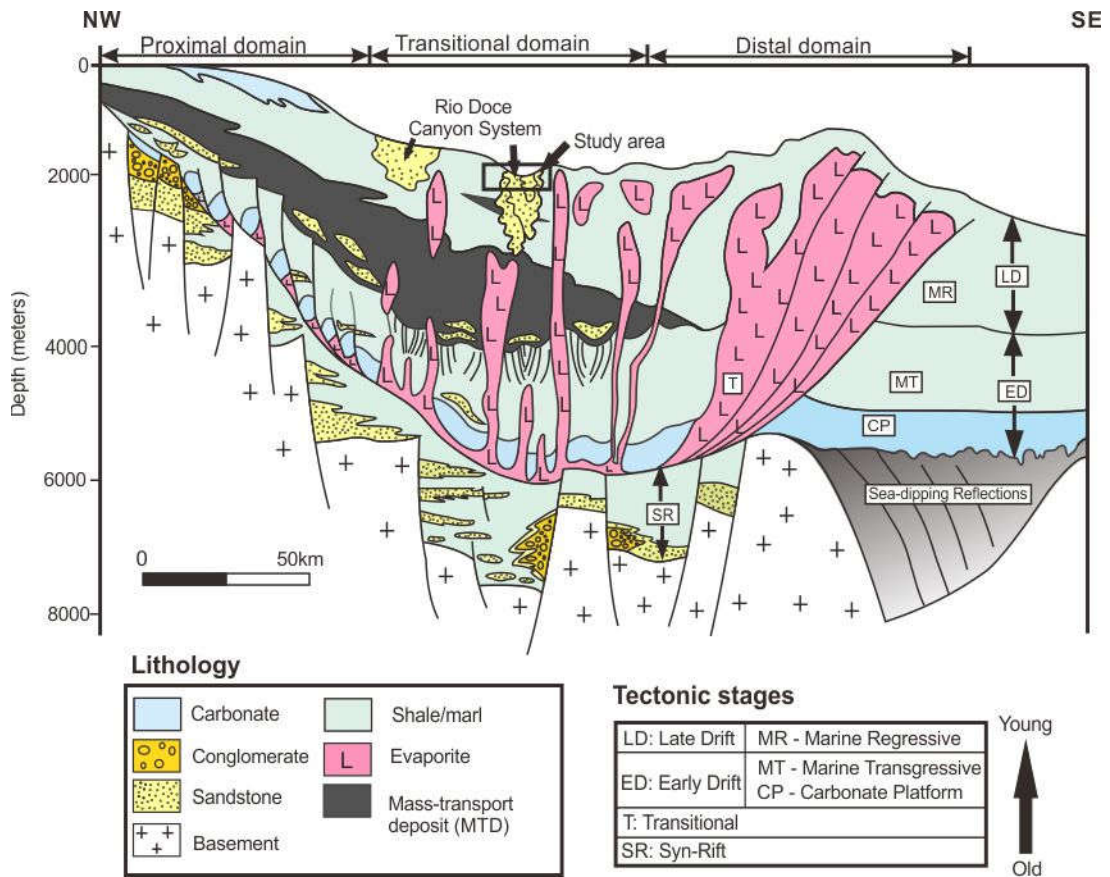


Fig. 4. Simplified regional cross-section across the Espírito Santo Basin showing major depositional sequences and salt tectonic domains. The location of the study area is indicated by the black box (modified from Fiduk et al., 2004 and Gamboa et al., 2010).

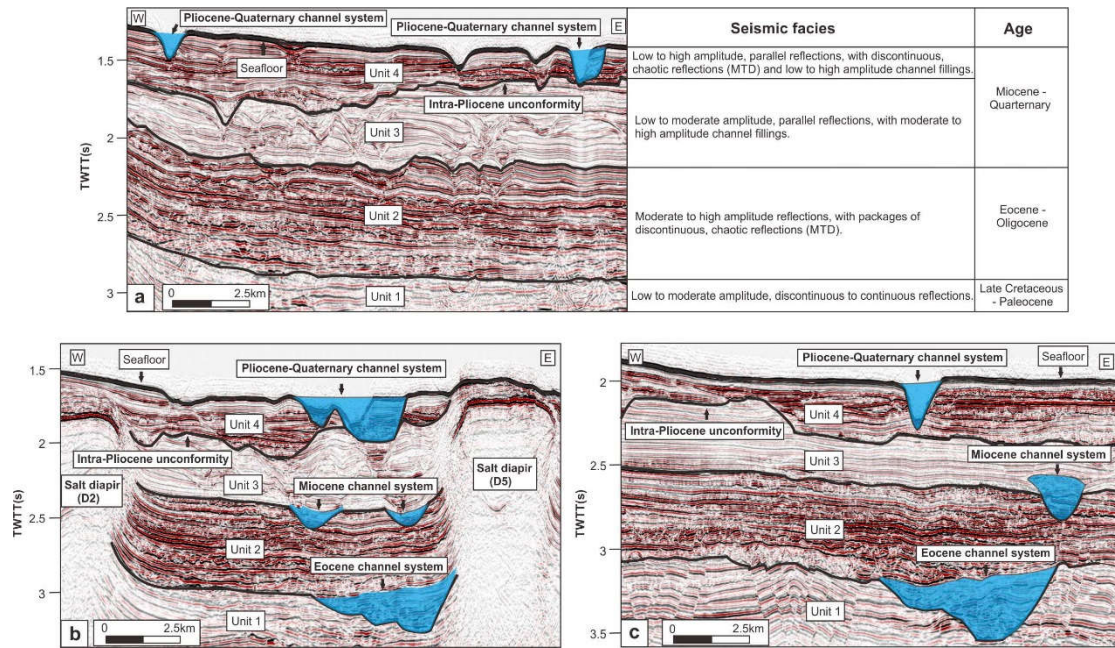


Fig. 5. Selected seismic sections highlighting the morphology of the Rio Doce Canyon systems. The location of the seismic sections is shown in Fig. 1b. Four seismic stratigraphic units are identified in the study area based on França et al. (2007) and Gamboa et al. (2012). The three main incision stages (Eocene, Miocene and Pliocene-Quaternary) recorded in the Rio Doce Canyon system are highlighted in blue on each seismic section.

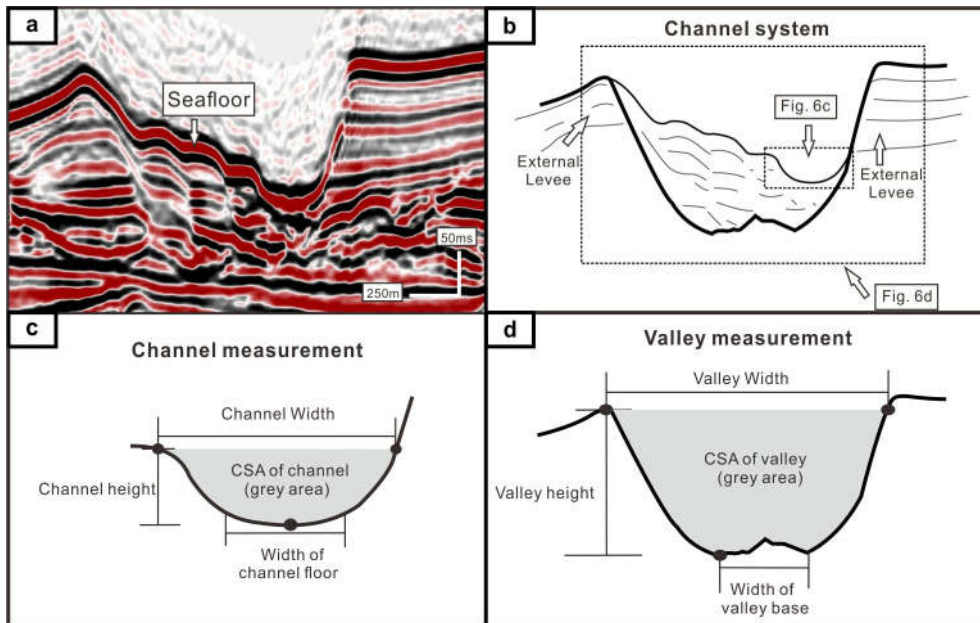


Fig. 6. Measurements taken for the Late Pleistocene-Holocene channel system interpreted in this work. (a) and (b) are uninterpreted and interpreted seismic sections of the channel system. (c) Channel measurements were taken along the channel axis and included the depth of the channel bank and thalweg, the width of the channel floor and the channel, and the cross-sectional area (CSA) of the channel. Channel height is the distance between the depth of channel bank and the thalweg. (d) Valley measurements were taken along the valley axis and included the depth of the valley wall and thalweg, the width of valley base and valley, and the cross-sectional area (CSA) of the valley. Valley height is the distance between the depth of valley wall and the thalweg.

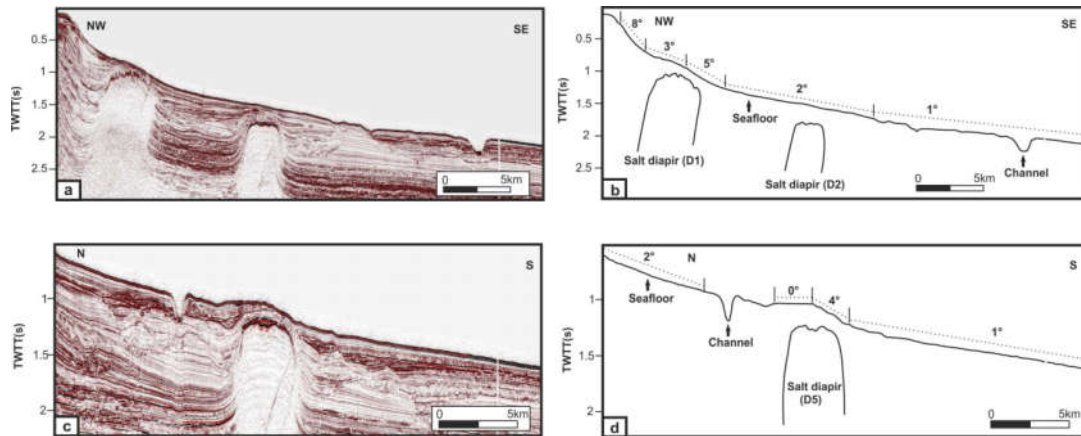


Fig. 7. Selected seismic profiles illustrating different seafloor slope trends in the study area. The location of the seismic profiles is shown in Fig. 1b. (a) Uninterpreted and (b) interpreted seismic profile showing decreasing slope trend in a NW-SE direction. Salt diapir D1 decreases gradient upslope and increases gradient downslope. Salt diapir D2 has a minor influence on the slope. (c) Uninterpreted and (d) interpreted seismic profiles showing decreasing slope trends in a N-S direction. Salt diapir D5 induces a decrease in gradient upslope and an increase in gradient downslope.

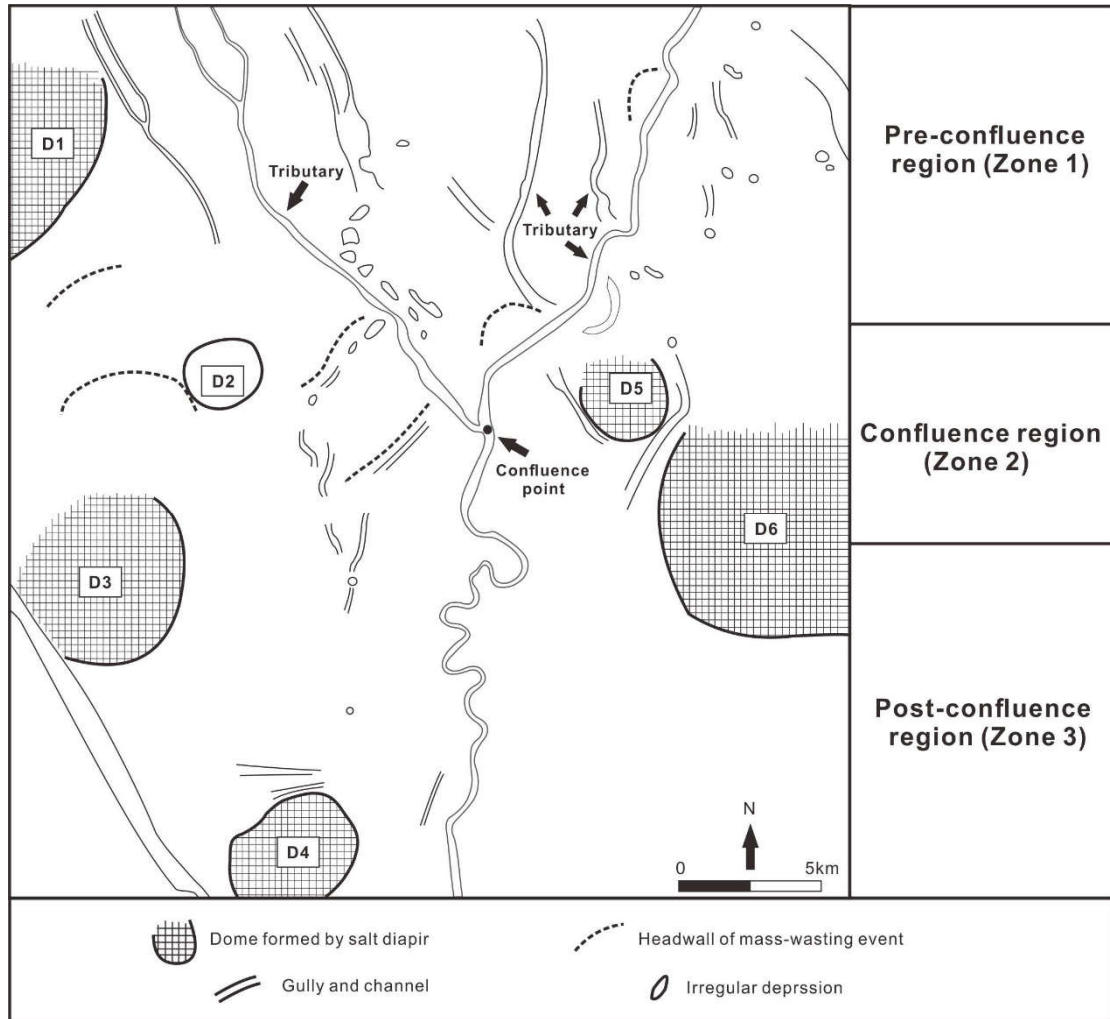


Fig. 8. Schematic representation of major seafloor geomorphologic features in the study area. The location of salt diapir D2 is shown, although no clear dome is presently observed on the seafloor in association with this structure. The pre-confluence and confluence regions show a variety of erosional features such as gullies, channels, headwall scars left by mass-wasting events and irregular depressions. In contrast, the post-confluence region is relatively smooth with fewer erosional features.

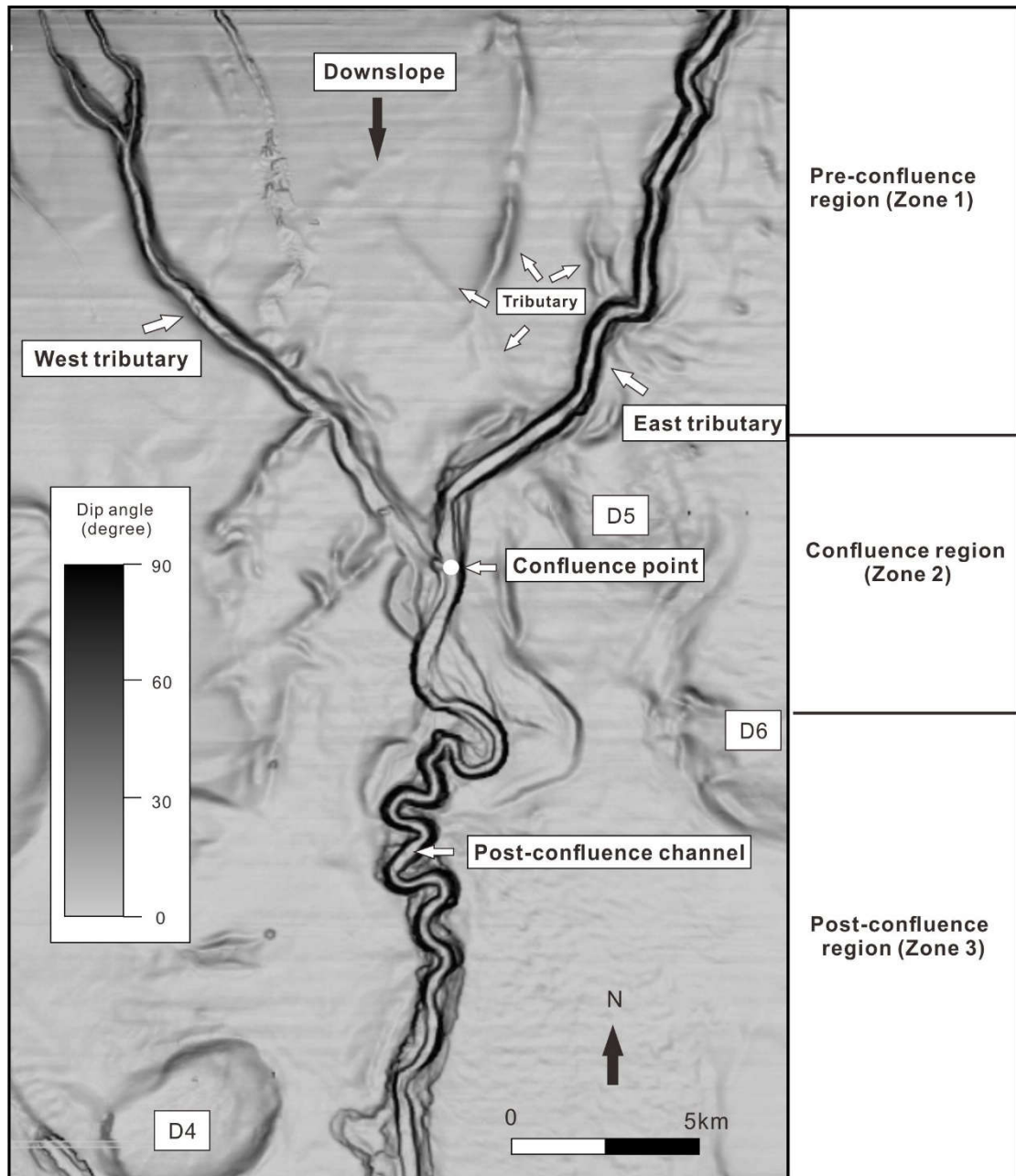


Fig. 9. Dip map of the seafloor showing that the seabed channel comprises west and east tributaries upslope and a post-confluence channel downslope. Other small tributaries connected to the east tributary are also observed on the seafloor. Both west and east tributaries change their orientation in the pre-confluence region, and were diverted into the confluence region due to the presence of salt diapirs. In the confluence and post-confluence regions, the general orientation of the channel changes to nearly N-S until the southern limit of the seismic volume is reached.

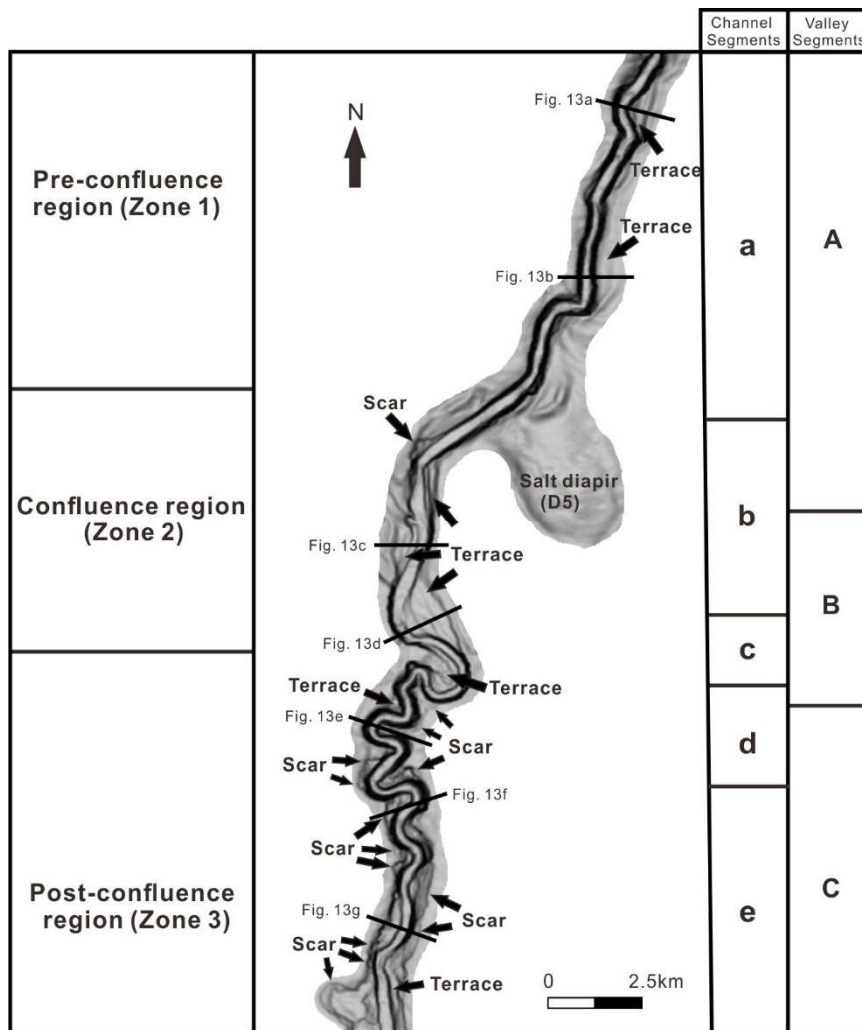


Fig. 10. Dip map showing the dominate sediment pathway of the channel system. The pathway is divided into different segments based on channel (Segments a to e) and valley dimensions (Segments A to C). Several terraces and scars are observed along the channel system.

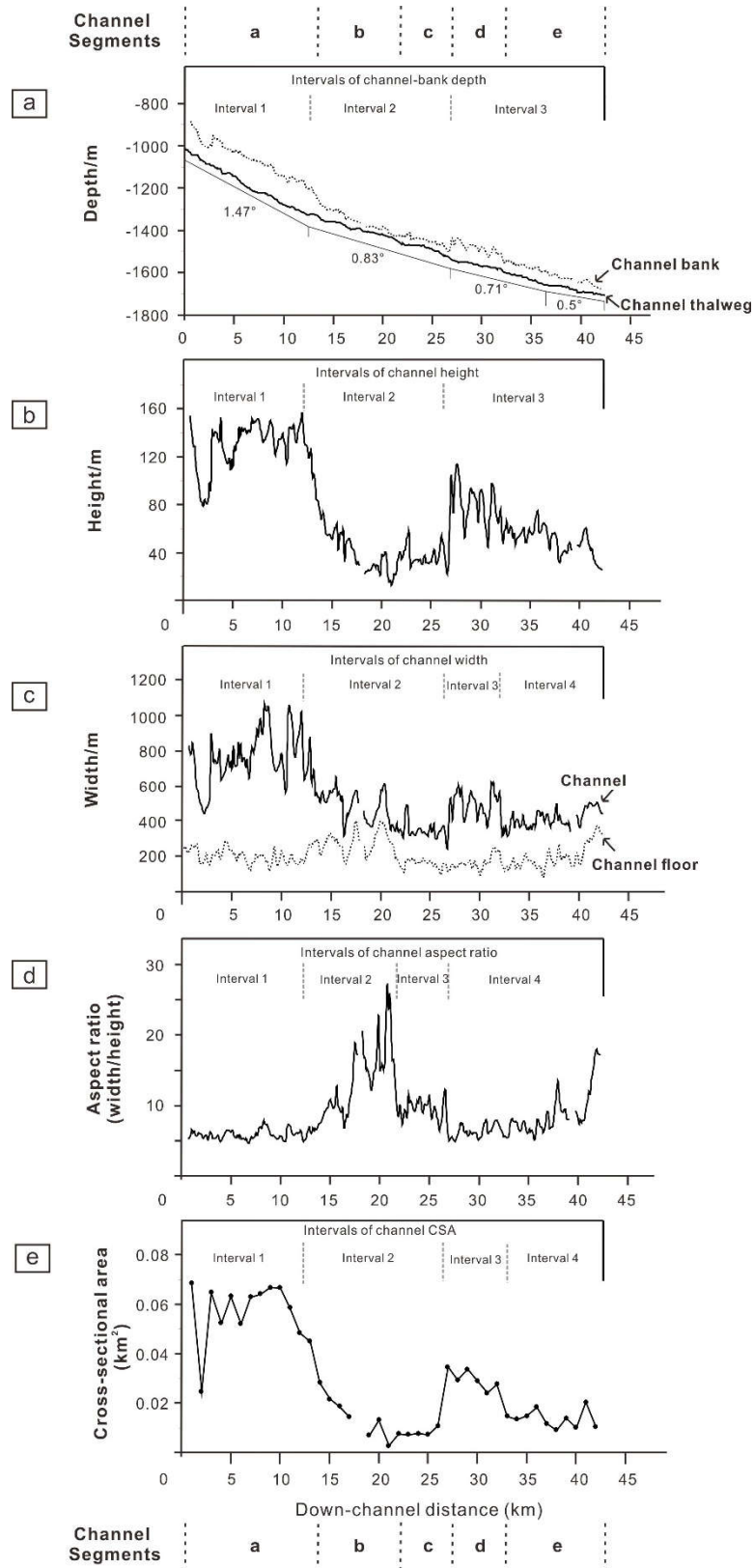

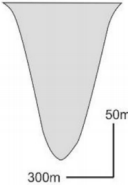
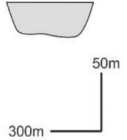
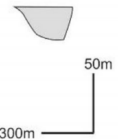
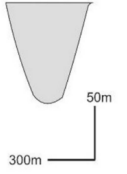
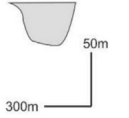


Fig. 11. Quantitative analyses of the channel. (a) Depth profile of the channel thalweg and channel bank. (b) Channel height profile. (c) Width of the channel floor and channel. (d) Aspect ratio (width/height) of the channel. (e) Cross-sectional area (CSA) of the channel.

Table 1. Summary of the morphological data acquired along the channel.

Measurements	Downslope 				
	Segments				
	a (0–13 km)	b (13–22 km)	c (22–27 km)	d (27–32 km)	e (32–42 km)
Channel gradient/degree	1.38°	0.89°	0.87°	0.65°	0.61°
Channel height/m (average)	129	42	38	80	51
Width of channel floor/m (average)	201	277	165	166	197
Channel width/m (average)	759	483	345	497	412
Aspect ratio (average)	6	13	9	6	9
CSA/km ² (average)	0.057	0.015	0.008	0.03	0.014
Examples of channel cross-section in each segment					

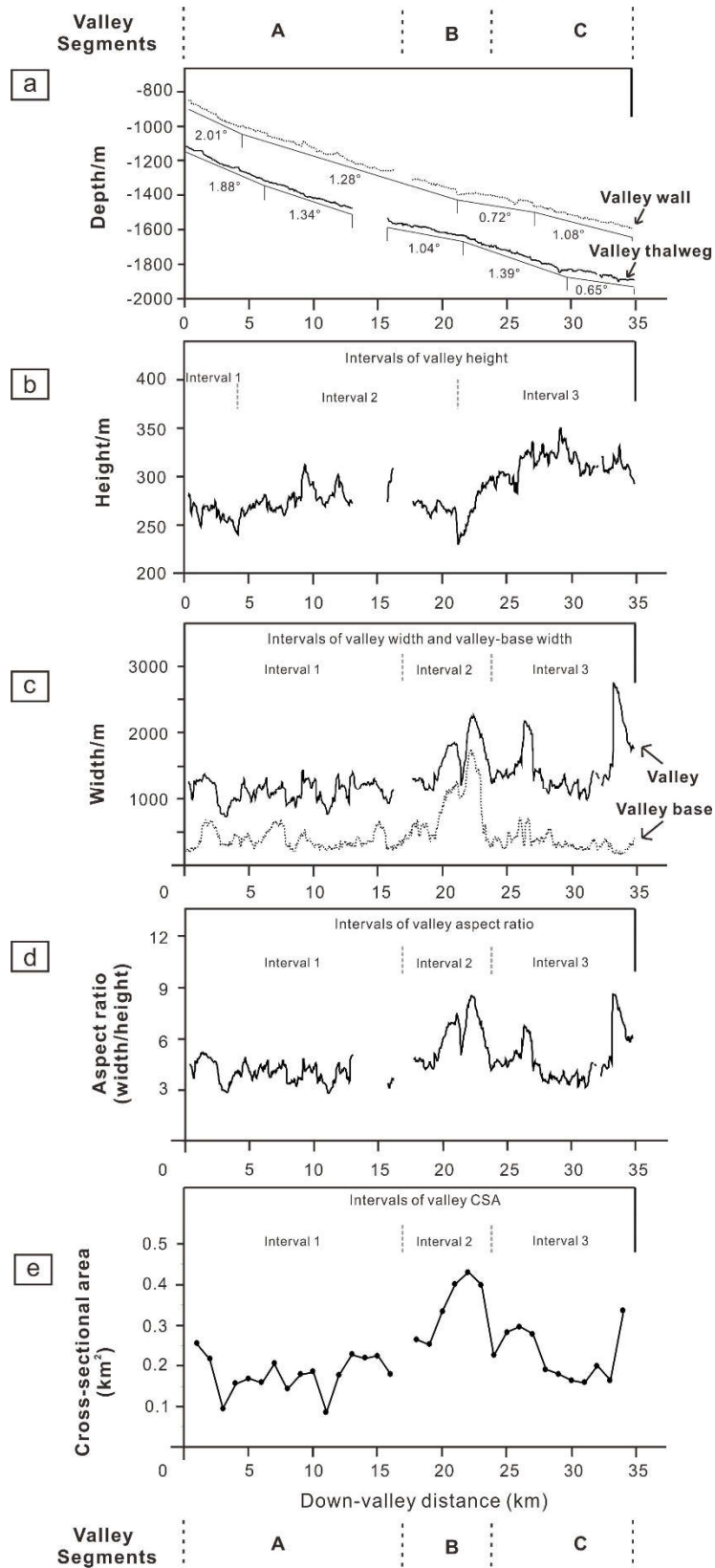

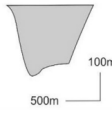
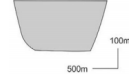
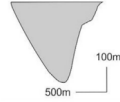


Fig. 12. Quantitative analyses of the valley. (a) Depth profile of the valley wall and thalweg. (b) Valley height profile. (c) Width of the valley base and valley. (d) Aspect ratio (width/height) of the valley. (e) Cross-sectional area (CSA) of the valley.

Table 2. Summary of morphological data acquired along the valley

Measurements	Downslope 		
	Segments		
	A (0–17 km)	B (17–24 km)	C (24–35 km)
Valley gradient/degree	1.51°	1.11°	1°
Valley height/m (average)	273	268	314
Width of valley base/m (average)	382	849	342
Valley width/m (average)	1117	1602	1495
Aspect ratio (average)	4	6	5
CSA/km ² (average)	0.181	0.348	0.226
Examples of valley cross-section in each segment			

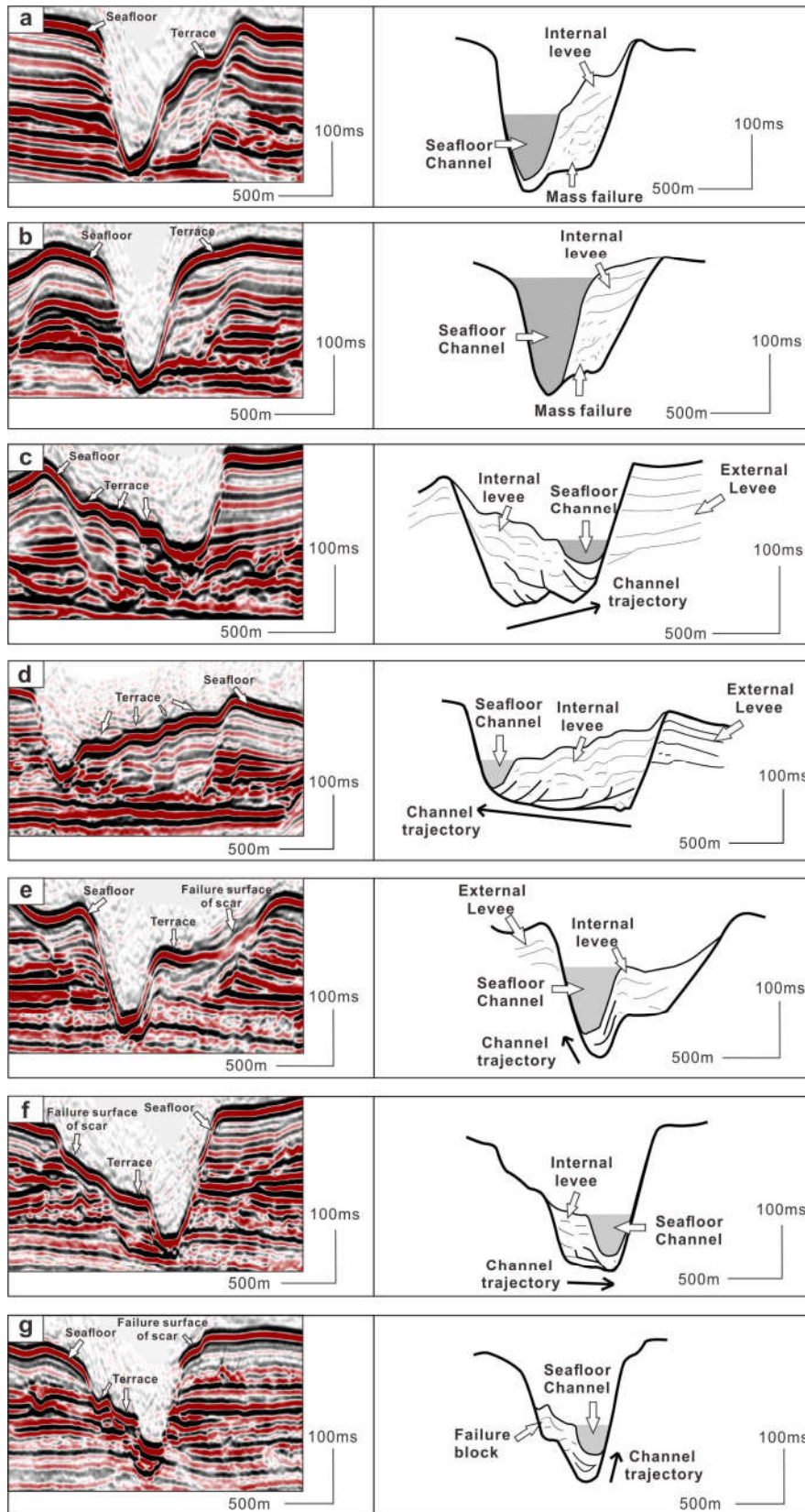


Fig. 13. Selected seismic profiles from each segment of the channel system.

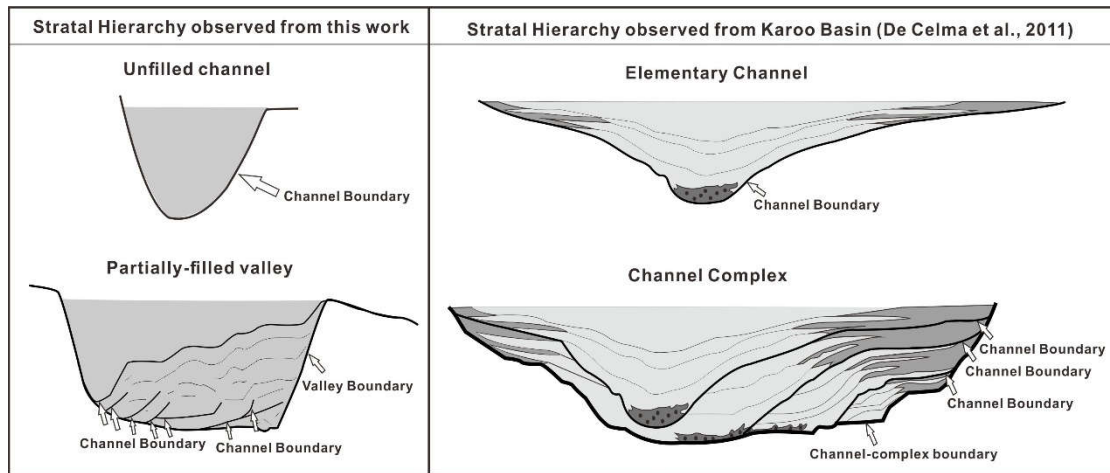


Fig. 14. Comparison between the stratal hierarchy in this study and outcrop data from the Karoo Basin, South Africa (Di Celma et al., 2011). The channel corresponds to the elementary channel of the Karoo Basin, both of which are fundamental elements of hierarchy framework. The valley correlates with the channel complex in the Karoo Basin, both of which were formed by lateral migration and the vertical stacking of channel elements.

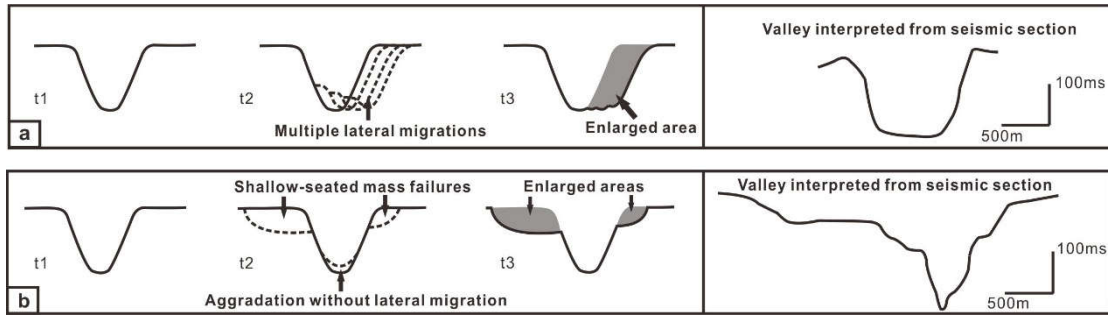


Fig. 15. Schematic diagram showing the effects of different erosional processes on valley morphology. (a) Cut bank erosion during lateral channel migration caused the retreat of the entire valley wall, leading to the widening of the valley, especially at the valley base. (b) Shallow-seated mass failures only enlarged the uppermost half of the valley wall.